TECHNICAL UNIVERSITY OF LIBEREC
Faculty of Mechanical Engineering

Assembling and testing of PIV system

Master thesis

Study programme:	N2301 – Mechanical Engineering
Study branch:	2302T010 – Machines and Equipment Design
Author:	**Chih-Hsiang Tsao**
Supervisor:	Ing. Petra Dančová, Ph.D.

Liberec 2018

DIPLOMA THESIS ASSIGNMENT

(PROJECT, ART WORK, ART PERFORMANCE)

First name and surname: **Chih-Hsiang Tsao**

Study program: **N2301 Mechanical Engineering**

Identification number: **S16000272**

Specialization: **Machines and Equipment Design**

Topic name: **Assembling and testing of PIV system**

Assigning department: **Department of Power Engineering Equipment**

Rules for elaboration:

1. Literature overview (principle of the method, state of the art, practical experiences with the method).

2. Description of experimental approaches used by different producers (e.g. Dantec, LaVision, TSI, and others).

3. Assembling of the experimental setup in stereo-scopic PIV.

4. Performing of the experiment.

5. Obtained data analysis and their comparison with literature.

6. Experiments recommendation for 3D PIV.

Scope of graphic works:

Scope of work report
(scope of dissertation):   approx. 40 pages

Form of dissertation elaboration: printed

Language of dissertation elaboration: English

List of specialized literature:

[1] Andreas Schroeder, Christian E. Willert, *Particle Image Velocimetry.* Springer-Verlag Berlin/Heidelberg (2008), ISBN 978-3-540-73527-4 www.dantec.com www.lavision.de www.tsi.com.

Tutor for dissertation: **Ing. Petra Dančová, Ph.D.**

                                  Department of Power Engineering Equipment

Date of dissertation assignment: **1 February 2018**
Date of dissertation submission: **1 August 2019**

prof. Dr. Ing. Petr Lenfeld
Dean

doc. Ing. Václav Dvořák, Ph.D.
Head of Department

Liberec, dated: 28 February 2018

Declaration:

I hereby certify that I have been informed the Act 121/2000, the Copyright Act of the Czech Republic, namely §60 – Schoolwork; applies to my master thesis in full scope.

I acknowledge that the Technical University of Liberec (TUL) does not infringe my copyrights by using my master thesis for TUL's internal purposes.

I am aware of my obligation to inform TUL on having used or licensed to use my master thesis; in such a case TUL may require compensation of costs spent on creating the work at up to their actual amount.

I have written my master thesis myself using literature listed therein and consulting it with my thesis supervisor and my tutor.

Concurrently, I confirm that the printed version of my master thesis is coincident with an electric version, inserted into the IS STAG.

Date: 21 / 5 / 2018

Signature:

Acknowledgement

First, I would hereby like thank my thesis tutor, Ing. Petra Dančová, who supports and gives advice on writing the thesis. Her guidance helped me in writing this thesis with useful comments and encouragement. Besides my supervisor, I would also like to express my very profound gratitude to the members in our department for assisting me and helping me in accomplishing the diploma thesis.

Abstract

In this paper, the main experiment is done by stereoscopic PIV and the result is analysed, including the formation of vortices that are observed, and the reconstruction images using Proper Orthogonal Decomposition (POD) method. Moreover, the planned future research is shortly described in the last chapter.

Appeared around 35 years ago, Particle Image Velocimetry (PIV) has been an essential measurement technique in fluid mechanics. Considerable efforts have been made to determine instantaneous velocity vector fields in a plane of the flow, which is the major asset of PIV. This technique measures the displacement of particles which are assumed to flow with the local flow within a given period of time. For evaluating the recorded images, the digital image is divided into smaller areas called "interrogation windows", sometimes overlapping between neighbouring areas, on which the cross-correlation function will be applied. However, the performance is greatly influenced by the preparation work in advance. Generally, the calibration plays an important role in this part. It requires taking several images of the calibration target within few parallel planes. According to these images, the "third axis" is computed by mapping function. By all means, the placement of calibration target should be aligned with the light sheet to minimize the possible error.

The evolution of PIV is still on-going as to capture dynamic velocity flow fields more precisely. Thanks to the progress in laser technologies and electronic imaging systems, the development of PIV technique is pushed further into next stage where measurement of velocity fields in three dimensions can be conducted. These 3D techniques include: holographic PIV, dual plane PIV, tomographic PIV. Tomographic PIV is built based on the concept lying in stereoscopic PIV; thus, the comparison between them is elaborated. The idea in calibration is similar, yet in 3D PIV polynomial calibration is used. Tomographic PIV is of course superior to stereoscopic in providing fully volumetric and truly instantaneous images and less sensitive to background noise. The entire targeted volume is focused by equipping a relatively small lens aperture under the Scheimpflug condition. In evaluation, the images recorded with two laser pulses are divided into small areas called "interrogation volume", on which 3D cross-correlation is applied. Also, 2C PIV is more sensitive to background noise and contamination on optical components such as dirt on vessel because of the lack of recoding cameras which can be used to compensate the image distortions. However, the drawbacks of tomographic PIV are the occurrence of ghost

particles and huge amounts of data that require large storage capacity. Thus, some algorithms are proposed to "digest" the enormous amounts of data. The "digestion" way varies in different producers for instance Dantec, LaVision, and TSI. These producers emphasized on different features. The tomographic PIV is produced by LaVision, so the DaVis software will be introduced in detailed. On realizing the fundamental concept in PIV, the future work will be continued right after the delivery of tomographic PIV.

Table of Contents

List of Symbols

E1	ground level
E2	excited level
h (J*s)	Planck's constant
v	photon's frequency
P_o	intersection of the object plane and optical axis
P_0'	intersection of the image plane and optical axis
P	any point in the object plane
P'	mapped point of P in the image plane
θ	angle between object plane and lens plane
α	angle between image plane and lens plane
a	coefficients of the polynomial
x	independent variable
y	dependent variable
I (x,y,z)	source function of the light intensity scattered by particles
μ	relaxation parameter
Wij	contribution of each voxel to each pixel
Ij	intensity of each voxel
Q	accuracy of the reconstruction
Ni	total number of pixels

Abbreviations, and Terms

DIC	Digital Image Correlation
BOS	Background Oriented Schlieren Technique
CCD	Charge Coupled Device
CMOS	Complementary Metal-Oxide Semiconductor
CID	Charge Injection Device
IPR	Iterative reconstruction of Volumetric Particle Distribution
FDM	Finite-Differences Method based
FVM	Finite-Volume Method based
LSM	Least Square Matching
POD	Proper Orthogonal Decomposition
OPD	Oscillating Pattern Decomposition
MART	Multiplicative Algebraic Reconstruction Technique
SMART	Simultaneous Multiplicative Algebraic Reconstruction Technique
MTE	Motion Tracking Enhancement
SMTE	Sequential Motion Tracking Enhancement
PPR	Primary Peak Ratio

1 Introduction

1.1   Background and development of PIV

A fallen leave floats together with the river, and sometimes sinks into the river: a simple phenomenon happening everywhere. One can easily observe the structures in the flow for instance swirls, water shoots, etc. This simple experiment allows human beings to observe the moving object in nature. Later in 1904, Ludwig Prandtl, who is often referred to as the father of modern aerodynamics, built up water tunnel to visualize and study the structures of the flow. Developed before PIV, Laser Speckle Interferometry was primarily established for the determination of displacement and strain in engineering structures. Speckle phenomenon is observed in early 60's. The speckle pattern consists of a variety of bright and dark spots where construction or destruction of incident light beam occurs, thus resulting in different irradiance levels. This technology introduces many advantages such as real-time visualisation and high radiometric sensitivity. Speckle pattern analysis also provides a wide variety of applications

For example, imaging, non-destructive testing, non-linear optics, and bio-speckle in the biomedical field. Thus, earlier researches refer PIV as "Laser Speckle Velocimetry". On the other hand, the trial and errors procedures are too long, and it is hard to reach the correlation theoretically. Hence, PIV system is invented with great advantage such as non-intrusive velocity measurement and whole field technique. Depending on the tracer particle density, three types of image density can be known, like particle tracing velocimetry, PIV, and "laser speckle technique".

Here, the development of PIV is focused. As mentioned above, the instantaneous measurement enables the wider usage of PIV in observing the velocity field within a very short time. The use of Nd:YAG (section 1.4.1) ensures the same, constant energy at any time delay between two pulses. Also, the removal of ambiguity often by image shifting increases the possibilities for PIV. Most importantly, the higher computer capacity of hardware contributes to great improvement for PIV data processing. Plus, the simulation of the recording and evaluation process are improved due to the basic understanding to PIV on the contrary to the complicated trial and error progress in the past. Other factors include the development of high-speed CMOS camera and higher repetition rate of lasers. as for details, a practical guide "Particle Image Velocimetry" by M. Raffel, C. Willert, S. Wereley, and J. Kompenhans give comprehensive source of information on PIV development.

1.2 **Related techniques**

Digital Image Correlation (DIC)

Digital Image Correlation (DIC) is an innovative non-contact optical technique and full-field image analysis method for measuring strain and displacement. Through comparing digital photographs of a component or test piece at different stages of deformation, in other words, based on grey value digital images, the contour and the displacements of objects under load in three dimensions can be measured. This method provides 2D and 3D deformation vector fields and strain maps. There are some advantages making DIC superior to speckle interferometry. First, the cost of DIC is lower than speckle interferometry. Second, complexity of speckle interferometry greatly restricts the usage. For DIC, outdoors usage is common as it does not require precise setup and low vibration environment. Last, like in other interferometry methods, the evaluation software of speckle interferometry cannot run completely automatically. The convenience of DIC let it develop faster and be applied more frequently for civil engineering.

Background Oriented Schlieren Technique (BOS)

BOS can also be called "white-light speckle density photography" as it uses white-light illumination and digital evaluation which are often used in its closet relative technique - speckle interferometry. However, the basic principle of this techniques is based on the relation between the refractive index of a gas and the density. Methods with local inhomogeneity in transparent media are frequently called schlieren (an old German word) techniques. Schlieren PIV is proposed by Settles (2010), using the turbulent eddies of a refractive flow as "particle" tracers. Thus, it is sometimes referred to "seedless PIV". The BOS method makes the process easier by replacing the laser-beam-generated speckle pattern with a random dot pattern on a surface in the background. Another advantage is the reduced requirements for optical access. F. Klinge et al. (2013) performed detected the wing tip vortex done by stereo BOS and stereo PIV at the same time. For many applications, a two-camera setup is sufficient to measure the position of flow structures in 3D; however, expending to multi-cameras is possible. With the increasingly usage of high intensity LEDs which level up the amperage to multiple times higher. As the result, exposure time is defined by the duration of light pulse instead of the shutter of cameras. In addition, the development of CMOs sensors and higher electronic storage devices, the recording and data process speed increase enormously. Recently, the research coupling BOS with other technique including PIV has been performed.

1.3   **Aim and scope of this thesis**

The purpose of this paper is to study the working principle behind PIV techniques as the preparation for further in-depth research in the future when tomographic PIV is delivered. Therefore, from the elaboration of each components of the system to the algorithm function behind the calculation will be briefly introduced first. To compare the performance, simple experiment should be done as in complicated experiment the influence factors and human errors would be induced, reducing the precision. After gaining the data from stereoscopic PIV, data should be processed to examine the quantitative result. Later, the advantages and disadvantages using this device should be discussed. Finally, as this study is to give readers some overview upon PIV techniques in order to operate the 3D PIV in the near future. This contains knowing the selection of particles and mixed it with working fluid in a proper density in each pixel, adjusting the multi-cameras in calibration as to reduce any possible errors, and being able to judge the reliability of outcome. The primary concern of this research is to organize the concepts in PIV techniques and basic operating skills as a stepping stone in the doctor's study which applies tomographic PIV in practice.

1.4 **Principle of Particle Image Velocimetry**

The Particle Image Velocimetry (PIV) technique provides a quantitative, instantaneous, whole-field visualisation. Furthermore, 3D PIV can describe the flow in three dimensions compared to conventional PIV technique which has just the description in two dimensional. This technique has a variety of applications, from slow flows conducted in laboratories to transonic and supersonic flows examined in industrial wind tunnels and turbine engines.

The principle of measuring the velocity is described as followed (Feng Bao et al. 2007). By adding non-toxic, non-corrosive, and chemically inert tracer particles in suitable density and diameter to the flow, in ideal condition, these particles move with the local flow without any interruption. Then laser beam from a (double) pulse laser adjusted by light sheet optics will then illuminate the flow where tracer particles are added. Within the extremely short time between two laser pulses, the light scattered by particles are to be recorded on a sequence of frames by cameras located perpendicular to the light sheet such as charge coupled device cameras or complementary metal-oxide semiconductor sensors. The recording is then divided in small subareas called interrogation areas. With the help of software, it analyses these interrogation areas to get the distribution of velocity vectors of cross-section area. The typical PIV system consists of some subsystems which are listed according to the importance.
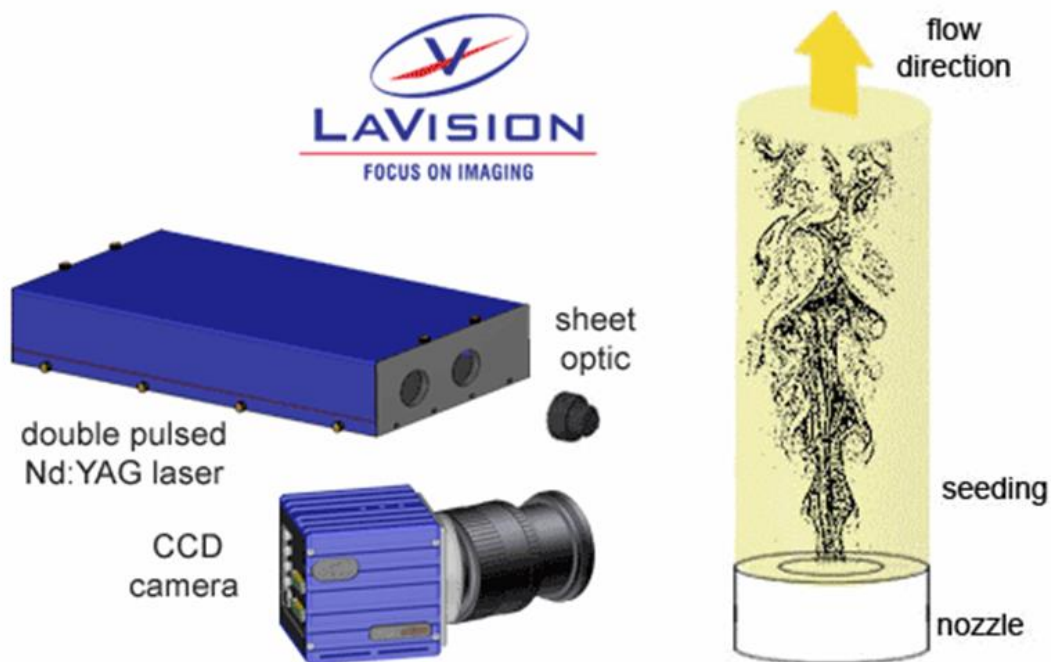

Figure 1 Experimental arrangement for PIV Picture courtesy of LAVISION found at
https://www.lavision.de/en/techniques/piv-ptv/

1.4.1 **Light sources**

Lasers are widely used due to its higher energy density. Argon-ion laser and Nd.YAG laser are mainly used because the sensitive wavelength of CCD and CMOS is near green light spectrum. There are three interactions between atoms and electromagnetic, such absorption, spontaneous emission, and stimulated emission. Generally, lasers belong to the last one. When the atoms in ground level receive specific energy (usually photon), they may be excited to higher level of state where it jumps back to the ground level by releasing energy.
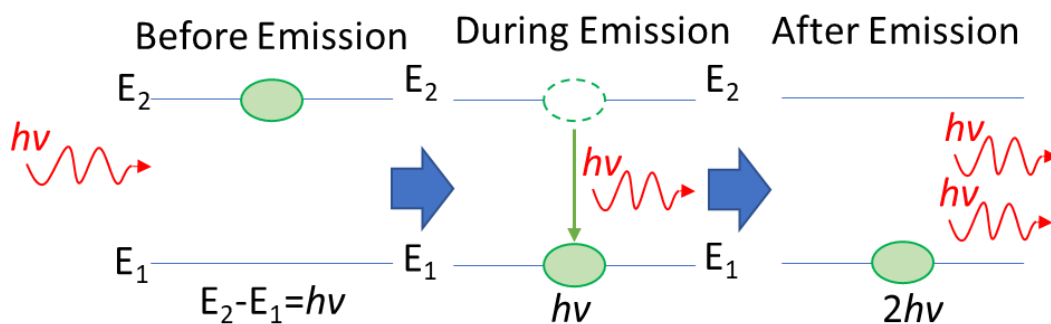

Figure 2 Stimulated emission,

where E2 is the excited level, E1 is the ground level, and *hv* is the energy used to "raise" atoms and be released during the emission.

Helium-neon laser

The helium-neon laser was built in 1961 by Ali Javan, Bennett, and Herriott at Bell Telephone Laboratories. Helium-neon lasers are the most widely used gas lasers and the most efficiency lasers in visible range. The helium-neon laser operates at a wavelength of 632.8 nanometers. Also, helium-neon laser emits light continuously, therefore, called continuous wave laser. The helium-neon laser comprises three essential components: high voltage power pump source, laser glass tube or discharge glass tube gain medium, and resonating cavity. Helium atoms absorb most of the energy supplied by the high voltage DC because the gas mixture is mainly made up of helium atoms. Helium atoms gain enough energy by the collision with electrons which are accelerated between the cathode and anode. As a result, helium atoms jump into excited states or metastable states. Helium atoms in these states collide with the lower energy state electrons of the neon atoms and transfer their energy to the neon atoms. Thus, helium atoms return to ground state while neon atoms jump into higher energy states or

metastable states. Compared with helium atoms, the metastable states of neon atoms have the longer lifetime. With more atoms remaining in metastable states, population inversion of neon atoms is achieved. This is the main pump mechanism.

Copper-vapor lasers

A copper vapor laser makes use of copper vapours as a lasing medium It produces green laser light at 510.6 nm and yellow laser light at 578.2 nm. Whereas most lasers are cool, copper-vapor laser needs thermal insulation because copper vapor is produced at 1500 °C. Vaporized copper atoms will obtain the energy by the collision with excited electrons and then will be excited to the upper states. Depending on level of state it reaches, the produced light for decaying from higher states emits different colours, either green or yellow. Overall, copper-vapor lasers have excellent power stability, good beam quality, and a long operational lifetime.

Argon-ion lasers

Argon-ion laser is a powerful gas laser with multiple watt of optical power in green or blue output light beam. The working principle is similar to the helium-neon laser. The difference is that during ionization and excitation, it needs high currents resulting in producing high power output. In addition, argon-ion lasers have higher gain system which is the measure of the ability of a laser medium to increase optical power. However, the construction of argon-ion lasers is difficult and costs more than He-Ne lasers.

Semiconductor lasers

Semiconductor lasers or laser diodes provide cheap and compact-size lasers. from the construction, there are mainly four kinds. First, single heterostructure replaces the homojunction with a heterojunction between layers of semiconductors with different composition improving the efficiency but only on one side. Secondly, double heterostructure replaces two sides with higher band gap material. Other two types are quantum well structure and vertical cavity surface emitting laser.

From the wavelength and its application, it can be divided into long wavelength (982 nm to 1550 nm) and short wavelength (300 nm to 950 nm). Among them, neodym- YAG lasers are worth mentioned because they are the most important solid-state laser for PIV.

In this experiment, FlowMaster Tomographic PIV bought from LAVISION company is expected to be used. It is equipped with EHP15-340-S-$\lambda\lambda\lambda$ laser from QUANTEL LASER. (see chapter 3)

1.4.2 **Light sheet optics**

What makes a lens different from any other transparent object is its ability to change the direction of light. Lenses are divided into two major categories called converging lenses and diverging lenses, respectively. The difference in structure lies in the thickness between that in the middle and at the edges as converging lenses are thicker in the middle than they are at the edges, while diverging lenses are in the opposite way. There are mainly three categories of lenses, cylindrical, spherical and cylindrical-spherical lenses (fig.3). Spherical lenses are those whose surface has the shape of the surface of a sphere while cylinder lenses refer to those with differing radii in the X and Y axe. In PIV technique, the tracer particles are illuminated with a thin light sheet, delivered from light sources through a combination of cylindrical lens which diverge light in one direction and spherical lens which waist light sheet. When the light sources such as argon-ion laser have sufficiently small beam diameter, one cylindrical lens is enough to generate the required light sheet, while some light sources such as Nd:YAG laser need additional lens. Usually, the diverging lens is set to be the first one to prevent the occurrence of focus line as the dusts around it may be ionized by high power lasers.
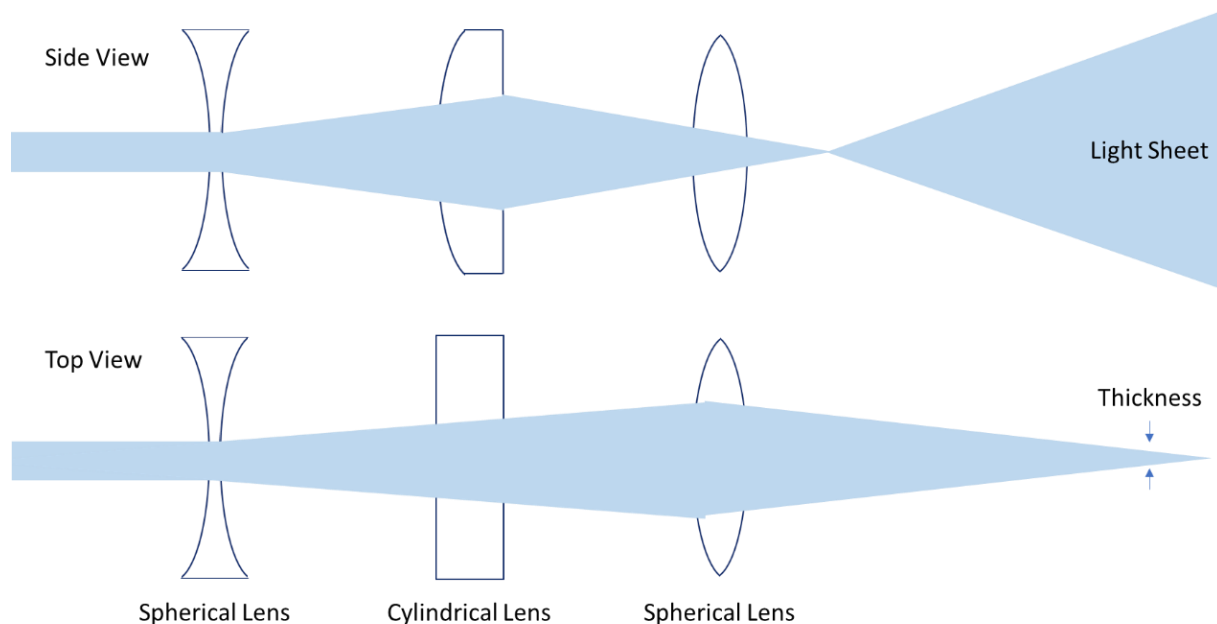

Figure 3 Light sheet optics

1.4.3 **Image Acquisition cameras**

PIV is an optical method consisting of recording images of illuminated particles within the flow-field. There is a variety of electronic image sensors and the most common ones are charge couple devices, charge injection devices, and complementary Metal-Oxide-Semiconductor.

Charge Coupled Devices (CCDs) were invented in 1969 at Bell Telephone Laboratories. CCDs are electronic devices which convert light into electric charge. The charges are converted to voltage levels, and then sent out as an analogue signal. This signal is then amplified and converted to numbers. The CCD structure consists of a two-dimensional array of metal-oxide-semiconductor (MOS) capacitors. When a bias voltage is applied to an electrode, a depletion region is formed in the semiconductor immediately beneath It. The charges are stored in the depletion region of the MOS capacitors. Charges are moved in the CCD circuit by manipulating the voltages on the gates of the capacitors and it's thus called "charge-coupled" device. In comparison, CMOS devices are more susceptible to noise. Light sensitivity is lower. CMOS devices consume little power as CCD devices need higher power to produce higher pixel quality. CMOS devices are cheaper and easier to manufacture. Unlike CCD cameras which transfer collected charge, the CID do not transfer the charge but 'inject' it into the substrate by reducing the electrode voltage to zero. By injecting the stored charge into the substrate, and by monitoring the current flow, signal readout is achieved.

	CCD	CMOS
Resolution	High	low
Light Sensitivity	High, plus single amplifier results in lower SNR	Susceptible to noise (often light hits transistors instead of photodiode, causing distortion)
Power Consumption	As much as 100 times more	Little (no extra applied voltage required)
Speed	High	Low
Cost	Expensive, but the technology is mature and stable	Manufactured on standard silicon production line, inexpensive

Table 1 Pros and cons of different image sensors

1.4.4 **Particles**

A PIV image is generated from the reflection of seeding particles in the flow field. They should also be small enough to be good flow tracers, yet large enough to scatter sufficient light for imaging. First, when adding particles to gas flow, hydroxyl functional group and lipid are used such as olive oil, tetraethyl orthosilicate, Ethylene glycol, Glycerol, and Di-Ethy1-Hexy1-Sebacat. On the other hand, when adding particles to liquid flow, the density of particles should be similar to the flow, but the diameter can be larger because of the better carry ability of liquid flow compared to gas flow. Some of the choices are hydrophilic aluminium powder, tapioca flour, and phosphor. On table 2, you can find the dimensions for commonly-used particles.

	Material	*Mean Diameter (μm)*	*Density (g/cc)*	*Refractive Index*
Dantec	Polyamide seeding particles	20	1.03	1.5
	Silver-coated hollow glass spheres (S-HGS)	10	1.4	-
	Fluorescent polymer particles (FPP)	10	1.19	1.479
LaVision	Graphite	3.5	2.2	-
	Ceramic hollow spheres (SC)	100	1.1	-
	PMMA	1 to 20	1.19	-
TSI	Polystyrene Latex (PSL)	0.54	1.05	1.55 to 1.6
	Titanium dioxide	3 to 5	4.2	2.6
	Hollow-glass spheres	8 to 12	1.05 to 1.15	1.5

Table 2 Common seeding particles

1.5   Literature Review (State-of-the-art)

Tomographic PTV, 3D-PTV, and defocusing PTV approach are assessed by Fuchs, Hain, and Kähler (2016). In their experiment, three-order polynomial approach is used as mapping function for tomographic PTV while camera pinhole model is utilized in 3D-PTV technique. These two different calibration functions result in the difference of measured value of maximum velocities. Due to the effect of scattering, defocusing PTV has higher z dependency of SNR. Thus, accuracy of particle image geometry determination is decreased as the elongated distance between illumination source and camera because same light intensity has to be distributed among the larger area on the sensor. In addition, the analysis of uncertainty of the main flow velocity in different axis is conducted. As mentioned above that the particle image diameter determination is more error-prone and less accurate as it's more away from the camera, hence, the uncertainty of the velocity measurement is larger. It is discovered that defocusing PTV shows the largest uncertainty which is around two times bigger. For tomographic PTV and 3D-PTV, the uncertainty is only slightly different but both approaches need at least two times the information to lower the uncertainty. In comparison to uncertainty in different axis, multi-camera approaches yield lower uncertainty in x and z direction where defocusing PTV has much more uncertainty. In y direction, due to the similar setup of defocusing PTV to 2D PIV, the uncertainty is much lower which is comparable to tomographic and 3D PTV. In conclusion, defocusing PTV generally has larger uncertainty than two other approaches but the cost is relatively lower, and it is easily to acquire the result; on the contrary, two other approaches need much more time to copy with complicated setup problems such as misalignment of cameras.

Sijie Fu et al. (2016) have compared the accuracy numerically and experimentally for indoor airflow study by 3D PTV and 2D PIV. As for numerical comparison of 3D PTV and typical PIV, tracking density plays an important role on the measurement accuracy and precision. It is shown that results from 3D PTV are biased when the density goes below 2. On the other hand, 3D PTV performs better than 2D PIV when the density goes beyond 3.5 or larger. Also, for larger displacement, 3D PTV provides more reliable results than 2D PIV. For experimental results comparison, PIV was unable to correctly measure low speeds of the order of 0.24 m/s. Except for that, measurements from two devices show certain agreement, yet the difference enlarges when air velocity decreases. It is concluded that tracking density has direct and important influence on these 2 devices. F.Alberini et al. (2017) conducted the experiments on comparison between 3D PTV and 2D PIV for determination of hydrodynamics. It is worthly

noted that for Newtonian and non-Newtonian fluids, average flow field captured by 3D PTV is comparable to that from 2D PIV while 3D PTV could not provide satisfactory result for turbulence flow. Overall, results from 3D PTV and 2D PIV have strong agreement.

Technique for the measurement of the flow field in a plane or volume is of importance in processing data. One of the most widespread techniques is digital particle image velocimetry (DPIV). With these techniques, quantities such as mean velocity and Reynolds stress distribution can be calculated. C. J. Kähler et al. (2012) compared three common-used evaluation methods, such as window-correlation method, single pixel ensemble-correlation, and tracking velocimetry (PTV). In their research, limitations for each technique are listed as followed, interrogation window dimension for window-correlation analysis, particle image diameter for single-pixel ensemble-correlation, and uncertainty in the estimation of the particle image position for PTV. It is concluded that based on the seeding densities, different methods should be applied. PTV is used in low seeding densities and non-constant flow gradients as in constant flow gradients, errors are averaged out. Four uncertainty quantification approaches were proposed and shared during LISBON SYMPOSIA events. These methods are uncertainty surface method (Timmins et al, 2012), particle disparity approach (Sciacchitano et al, 2013), peak ratio approach (Charonko and Vlachos, 2013), and correlation statistics method (Wieneke and Prevost, 2014) respectively. To test the efficacy of PIV uncertainty methods, experimental database was established in D. R. Neal et al. (2014) within the conference. PIV-HDR" (high dynamic range) system was used in comparison with hot-wire anemometer (HWA) system and PIV system. The result from PIV-HDR system exhibits three to fourfold higher accuracy than the PIV-Measurement system which has a high correlation to that from HWA system. For evaluating PIV uncertainty quantification methods, the synthetic data was utilized, and correlation statistics and particle disparity approaches were found to have the consistent uncertainty distribution as the real error. Besides, B. Wieneke (2014) adopted particle disparity method but operates on a pixel level instead. It shows good agreement with the true random error in most cases.

Techniques for measuring velocity by PIV have been developed. It includes the method of Glowinski and Pironneau by L.K Waters et al. (2004), describing and analysing the Glowinski Pironneau method for the unsteady Stokes problem. Based on a generalization of the Glowinski–Pironneau method for the uncoupled solution of the incompressible Navier–Stokes equations, F. Auteri et al. proposed a new method to compute the pressure field in comparison with Navier–Stokes equations as well as those methods developed from it. The proposed

method is then compared with other methods for example, Poisson problem for pressure in conservative formulation. Finally, the proposed method is tested with oscillating airfoil, showing promising result.

In order to evaluate time-resolved three-dimensional data, conventionally there are two domains: tomographic-PIV and 3-dimensional PTV. Ralph Lindken et al. compare results from data recorded with a stereomicroscope between 3D-μPTV and tomographic μPIV. They indicate that for the in-plane components, these two methods have good agreements. However, in lower seeding density, 3D-PTV yields precise results; on the other hand, tomographic PIV can process flows with higher seeding densities which is around one order of magnitude high but the whole processing is computationally costly. However, ghost particles influence the velocity vector result and Cross-correlation is needed. In addition, large amount of data needs to be save in hard disk and generally long computational time is required. Alternative particle detection methods such as Iterative reconstruction of Volumetric Particle Distribution (IPR) is performed but the problem remains as the particle image density approaches 0.05 ppp.

Thus, a novel approach called "shake the box" is proposed and evaluated. This approach assumes that for a certain number of time-steps, the trajectories of almost all particles are known. Therefore, the initialization of track system is an important step. This process determines the trajectories of the first four time-steps. Based on it, the next time-step is predicted. Then the particles will be "shaken" or moved to the predicted position, that is, from residual images into optimal position. The predicted particle positions will be close to the real ones. The whole position refinement (Daniel Schanz et al. 2016) includes initial shake, intensity correction, deleting particles, and identifying new particle candidates. Later new particles entering the measurement zone will be detected and shaken as depicted above while the residuals of the tracked particles vanish, leaving new particles to be detected. It is worth noting that the complete elimination of residual can only be achieved by using synthetic data. This process can last more than 4 times if necessary. For low to moderate seeding densities, the algorithm needs very little convergence time; however, for high seeding densities (0.125ppp), more errors occur and needed to be corrected, so the algorithm needs 25 time-steps to converge, and above these seeding densities, no convergence can be achieved now. By the mentioned approach, the ghost level is remarkably reduced mainly because of the "prediction" step. "Shake-The-Box" was specifically designed to incorporate with other temporal and spatial information. To further reach the lower ghost level, several ways have been examined for instance, shorter time-series

and IPR introduced by Wieneke. Among the applied method, four-pulse TOMO-system has shown the best ability to predict the trajectories.

After the requisition of data, reconstruction of the particles shall be reformed (section 2.3.2). There are several techniques such as Algebraic Reconstruction Technique (ART), Simultaneous Algebraic Reconstruction Technique (SIRT), Simultaneous Multiplicative Algebraic Reconstruction Technique with Correction (SMART). These techniques can be summarized basically in four steps: creation of the initial image, calculation of corrections, patches and application of the convergence test. Multiplicative algebraic reconstruction technique (MART), depicted in Eric F. et al. (2011) research, is a similar approach with correction factor to ART. Timothy W. et al. (2015) have proposed a new method based on the well-known computational refocusing, which is said to be orders of magnitude faster than MART and doesn't require large amounts of memory or hard drive space for its execution. This method describes that points in the focal stack will only be assigned a non-zero intensity if a minimum percentage of the light rays passing through that point have a recorded value above some minimum threshold, otherwise particles are assumed not existing. With this method, similar accuracy is achieved with orders of magnitude less computational time.

N. J. Neeteson et al. extracted pressure fields with two techniques: Eulerian and Lagrangian. It is found in their work that Lagrangian technique shows better performance under Dirichlet boundary conditions while worse estimates are produced under Neumann boundary conditions. Historically, Eulerian flow measurement is applied in terms of spatial resolution and great majority of velocimetry-based pressure measurement. In Eulerian domain, the construction of a network is formed by simply connecting neighbouring points resulting in equal shape functions and cubes with same side lengths. Conversely, an unstructured Lagrangian network produces non-unity shape functions and multi-faceted control volumes. In recent years, Lagrangian measurement techniques have been investigated rapidly. N. J. Neeteson et al. compared Eulerian Pressure Extraction, finite-differences method-based, Lagrangian pressure-extraction technique (FDM), and finite-volume-method-based, Lagrangian pressure-extraction technique (FVM). Same boundary conditions are used in three methods. Lagrangian FVM outperforms than two other methods. Lagrangian FVM is found to be able to capture the pressure maximam with nearly an order of magnitude less error than Eulerian Pressure Extraction. Lagrangian FVM also eliminates the sensitivity to pressure gradients on the boundary which Lagrangian FDM finds it difficult. Tomopgraphic PIV utilizes Eulerian technique which exhibits more errors compared to Lagrangian. Despite the fact that Lagrangian

pressure-extraction technique is superior to existing Eulerian techniques under Dirichlet boundary conditions, Lagrangian pressure-extraction techniques still need more investigation and improvement, especially under Neumann boundary conditions.

2 Theory

This paragraph includes basic introduction of optical theories and calibration method for tomographic PIV and stereoscopic PIV. Also, the layouts of softwares are shown.

2.1 Theory of stereoscopic PIV

With the stereo arrangement of two cameras from two viewing directions, images of particles within light sheet are then taken. From these images, three dimensional vectors are measured. Stereoscopic PIV is widely used because of the following reasons. It eliminates the perspective error inherent in conventional PIV which uses single camera oriented orthogonally to the illuminated plane. Conventional PIV can measure out-of-plane velocity components and those occur to contaminate the in-plane components. Therefore, full velocity vectors can be observed from two simultaneous views. Secondly, the cost is comparatively fair contributed mainly from one extra camera and complex software to process the data.

There are two configurations of stereoscopic PIV system (fig.4), such as angular displacement and translation configuration.
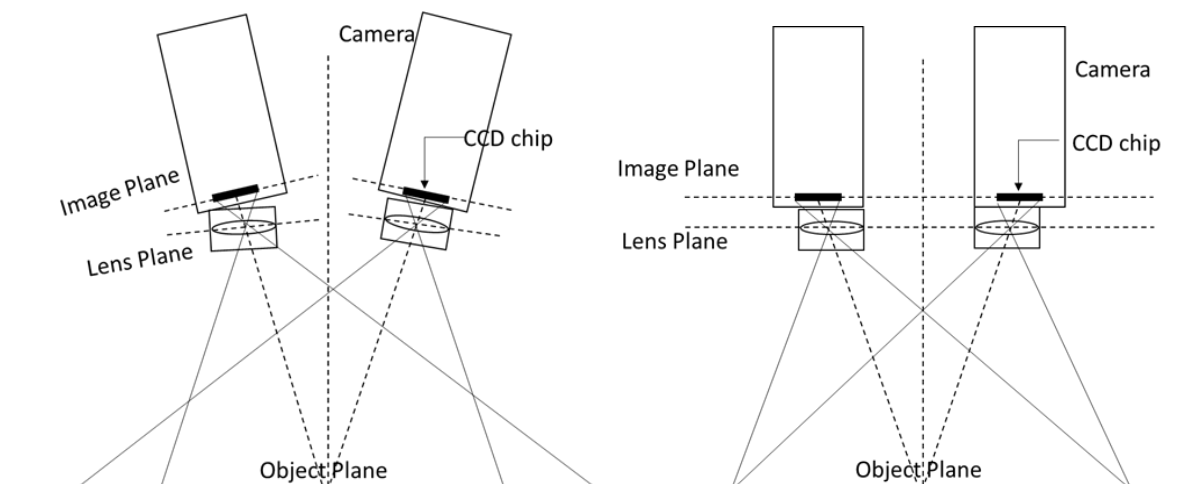
Figure 4 Two Configurations of stereoscopic PIV system

2.1.1 **Angular displacement**

The geometrical arrangement of angular displacement follows *Scheimpflug condition* assuming lens are distortion-free. It consists of two parts. First, three planes must have one intersected point. Second, the intersected point of object plane and optical axis, point P_0, must be imaged to image plane P_o'. Instead of utilizing this condition, another simple solution to get well-focusing particle images is to increase the depth of field of the recording optics.
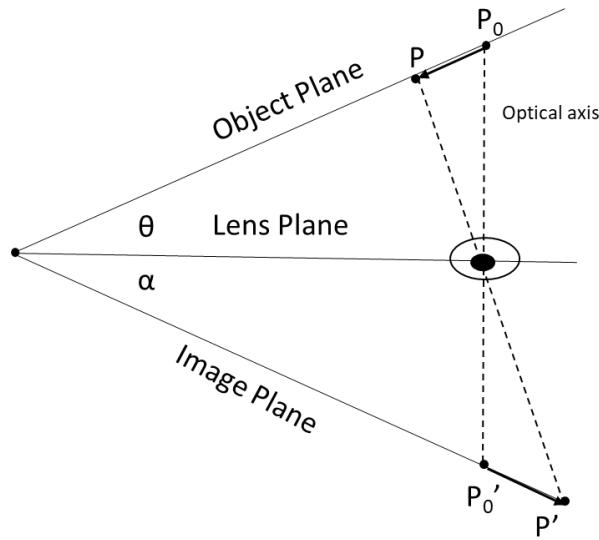
Figure 5 Schematic of Scheimpflug condition

In angular system, the object plane is not paralleled to the lens plane; however, the optical axes of the imaging lens are tiled at an angle that imaging can remain paraxial for any value within stereoscopic viewing angle. There exists some small angle between image plane and lens plan, but the impact generally is determined during the installation of the optical system. Thus, the imaging does not suffer from strong optical aberrations.

Although under Scheimpflug condition wider image area could be achieve, images may have some influence from distortion. While using the high precision stereoscopic PIV is used, the proper calibration with respect to it must be applied.

2.1.2 **Translation displacement**

In comparison to angular system, translation system is simpler. The optical axis of the imaging lenses is parallel to the object plane. The main advantage of translation configuration is that the accuracy and the precision of the measured displacements are uniform from the entire image domain unlike the distortion displacements in angular system. The images can be applied without remapping. Nevertheless, the disadvantage of translation configuration is that the range of stereoscopic angle is limited, which is considerably small than the one in angular system. With current techniques, the procedures to remap and calibrate the data from angular configuration are well-developed, so the angular displacement configuration is primarily used.

2.1.3 **Calibration for stereoscopic PIV**

Accurate calibration plays an important role in reconstruction of three-component displacement vectors. In general, the calibration target should contain enough number of markers on it, typically 10-20 in each in-plane direction. The procedures for calibration is described below, which are quoted from the product-manual. The procedures are very similar to that of stereoscopic-PIV, except the step to apply the third-degree polynomial function (from product manual).

   (i)   Place the calibration target at the centre of light sheet

   (ii)   Record the image at this position and set it as benchmark

   (iii)   Compare the known markers with corresponding marker positions on each camera image (with the help of correlation function of the software)

   (iv)   Use the benchmark whose position is known to find out the four markers around it and after the spacing between them are calculated, based on these newly-calculated markers, repeat this step

   (v)   Apply third-order polynomial function for x and y variables in images of all marks in calibration target (Soloff et al. 1997)

$$F(x)=a_0+a_1x+a_2y+a_3z+a_4x^2+a_5xy+a_6y^2+a_7xz+a_8yz+a_9z^2+a_{10}x^3+a_{11}x^2y+a_{12}xy^2+a_{13}y^3$$
$$+a_{14}x^2z+a_{15}xyz+a_{16}y^2z+a_{17}xz^2+a_{18}yz^2 \tag{1}$$

   (vi)   Move the calibration target in the direction normal to the calibration target (at least three planes are needed to determine the mapping parameters)

2.2 **Theory of tomographic PIV**

Tomographic PIV provides the possibility to measure particle motion within a three-dimensional measurement volume thanks to the development of tomographic algorithm technique (fig.6).

Tomographic PIV overcomes the shortcoming of stereoscopic PIV that it cannot capture a complete volume. However, some limiting factors determine the implementation of tomographic PIV. For example, higher power (generally 5 higher time than that for stereo PIV experiment), longer digital evaluation of recordings, and larger data storage (generally 10 times larger than that for plane PIV) are required.
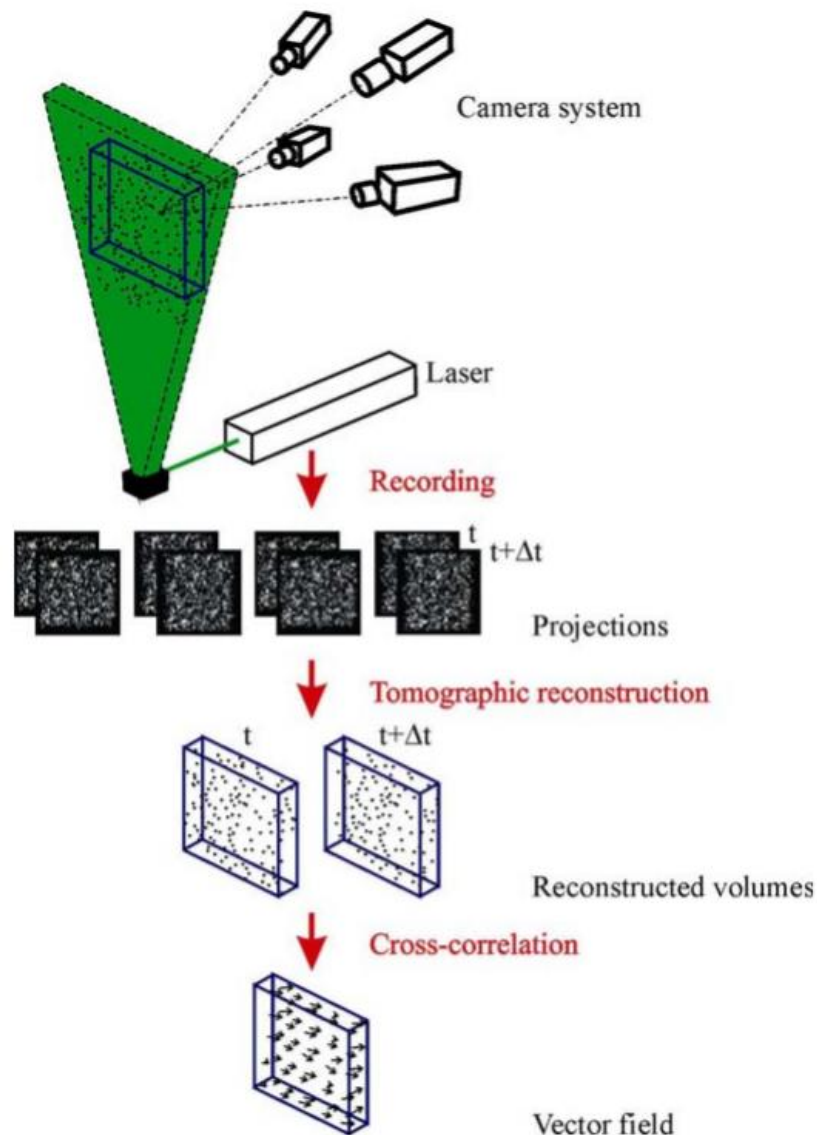
Figure 6 Tomographic particle image velocimetry G.E. Elsinga, F. Scarano et al. (2005)

2.2.1 **Tomographic reconstruction algorithm**

The intensity of each pixel Pi in the series is recorded along its line-of-sight through the volume as drawn below.
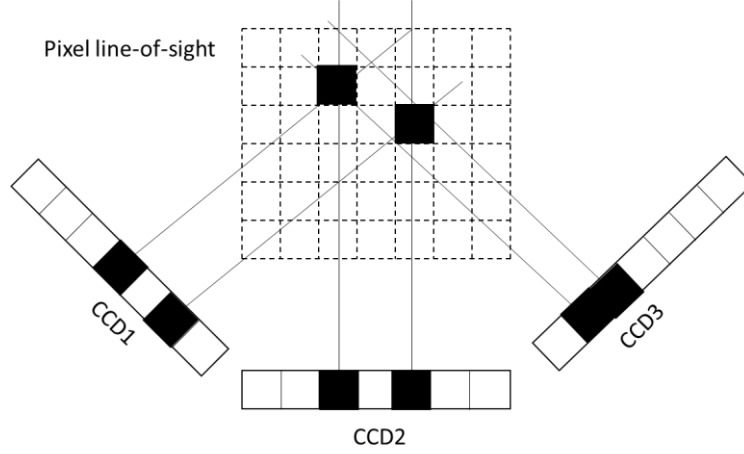
$P_i = \int_{-\infty}^{\infty} I(x,y,z)\, ds_i$, where $I(x,y,z)$ represents the source function of the light intensity scattered by particles. Several algebraic methods are capable of solving this equation, for instance, algebraic reconstruction technique (ART) and multiple algebraic reconstruction technique (MART).

ART:

$$I^{k+1}(X_i, Y_j) = I^k(X_i, Y_j) + \mu w_{ij} \frac{P_i - \sum_{j \in N_i} w_{ij} I^k(X_i, Y_j)}{\sum_{j \in N_i} w_{ij}^2} \tag{2}$$

MART:

$$I^{k+1}(X_i, Y_j) = I^k(X_i, Y_j) \left(\frac{P_i}{\sum_{j \in N_i} w_{ij} I^k(X_i, Y_j)} \right)^{\mu w_{ij}} \tag{3}$$

, where μ is a relaxation parameter typically chosen between 0 and 2, w_{ij} (weighting matrix) that represents the contribution of each voxel to each pixel, and $I(X_i, Y_j)$ represents the intensity of each voxel.

$$Q = \frac{\sum I_{real} * I_{reconstruction}}{\sqrt{\sum I_{real}^2 * \sum I_{reconstruction}^2}} \tag{4}$$

The reconstruction quality factor Q indicates the accuracy of the reconstruction, which is computed as the normalized cross-correlation coefficient between the true solution and the reconstructed intensity field.

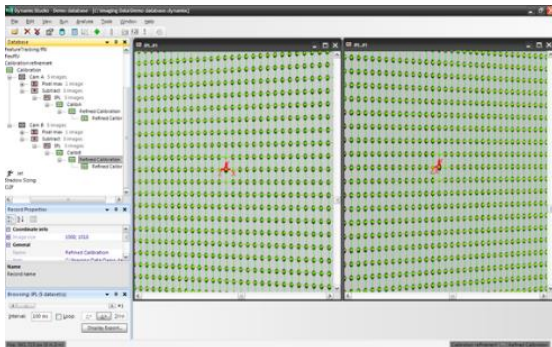*Formation of ghost particles*

In typical tomographic PIV, limited projections lead to non-unique solution to the algebraic reconstruction. Particles formation at the intersections of lines-of-sight from each camera corresponding to actual particles may contain the so-called "ghost particles", which introduce errors in the consequent cross-correlation and ultimately have a great impact on the velocity fields. With more lines-of-sight intersections, recorded ghost particles increase. A simulacrum matching-based reconstruction enhancement (SMRE) technique is proposed to reduce ghost particles in a reconstructed intensity field. SMRE utilizes the characteristic shape and size of actual particles to remove ghost particles in the reconstructed intensity field (C M de Silva et al. 2013).

2.3   Experimental approaches by different producers

This section focuses on the feature functions that each software from different producers can achieve in the field of fluid mechanic. DynamicStudio accommodates a range of methods and techniques for image measurements with easy set-up. The measurements include four main categories such as volumetric particle image velocimetry, planar particle image velocimetry, particle characteristics & spray diagnostics, and combustion diagnostic& mixing. DaVis 10 features in its ability to process data of 4D measurements of flow fields, 3D surfaces, sprays, mixing and combustion processes. Insight 4G software can also perform particle image velocimetry and planar laser induced fluorescent related researches. All the software makes advanced imaging measurements easier and provides cutting-edge innovations in laser image area.

### 2.3.1 **Dantec - DynamicStudio software (stereoscopic PIV)**

The following picture (fig.8) demonstrates the interface of DynamicStudio software in stereoscopic PIV. The procedures include camera calibration, calibration refinement, 2D vector maps calculation, and evaluation. After the data is obtained, several modes for processing data are introduced below, including Least Square Matching, Proper Orthogonal Decomposition, and Oscillating Pattern Decomposition.
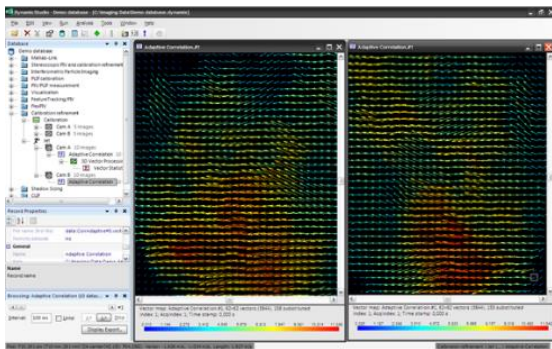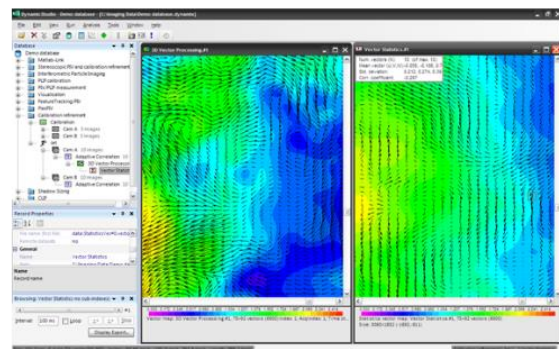

Figure 8 Interface of the software from Dantec Dynamic website

Least Square Matching (LSM)

LSM is one of the image matching techniques targeting on finding the corresponding pixel on two images of the same physical region (Zeyu Li et al. 2014). That is, LSM uses a model to describe the movement of fluid elements. LSM method obtains the velocity gradients directly, offering reliable information with no need to differentiate the velocity field. However, LSM is subject to the divergence problem, for example systematic errors (initial bias) and outliers

(imaging sensor malfunction). The previous one makes it harder in practical use because of the difficulty in estimating the initial value. If these biases are high enough, solution may be divergent. The errors should be corrected by a stricter threshold of inliers and outliers. The later shortcoming relates to faults in the imaging sensor. A few pixels in image acquisition sensor does not function properly, resulting in dead or stuck pixels on the generated image. This weakness of LSM should be taken into account and be solved by various filters such as mean filter, Gaussian filter.

Proper Orthogonal Decomposition (POD)

POD is a powerful method of data analysis. It is extensively used in image processing, signal

analysis and data compression (Anindya Chatterjee 2000). It helps to gain the low-dimensional descriptions from high-dimensional data. However, POD is sensitive to coordinate changes and its failure on distinguishing between a featureless cloud of points on some plane. In general, POD extracts typical coherent flow structures from PIV data and is helpful in dealing with high-dimensional data.

Oscillating Pattern Decomposition (OPD)

OPD provides information related to the stability of the flow. OPD defines modes according to their stability properties while POD arranges modes by its energy content. OPD is favourable when the identification of wavy structures is needed. However, OPD can only be applied on time–resolved data. Very often OPD is compared with POD mentioned above. Since POD is based on spatial correlation and OPD is based on temporal linear evolution dynamics. Besides, OPD can retain phase information and modal growth information, which are superior to POD analysis as long as the time-resolved data is sufficient for OPD.

2.3.2 **Lavison DaVis tomographic PIV software**

DaVis is the software excellent at advanced image processing algorithms, intelligent storage and presentation of multi-dimensional image data. This section is the brief introduction of usage of software from product manual from LaVision about how to setup the parameter or functions to process the required data, especially in 3D PIV.

Image pre-processing

This step is to eliminate or reduce the influence from camera background and camera noise. These methods are dictated as followed, *subtracting sliding minimum* to remove the image background, *normalizing with local average* to equalize the particle intensity on a larger scale, *gaussian smoothing* to increase the particle size, and *using mask* to get rid of reflections due to the uneven illumination. However, if noise is still obvious, applying *sharpening* or *subtract constant from each pixel* after gaussian smoothing can be helpful in reducing the noise. During these steps, the intensity of the particles may be much reduced, so *multiplying each pixel with factor* can be of use.

Volume self-calibration

In this step, the disparity vectors are calculated and then used to correct perspective calibration.

Above: no volume self-calibration, no vector post-processing, color = V_z

volume self-calibration, no vector post-processing, color = V_z
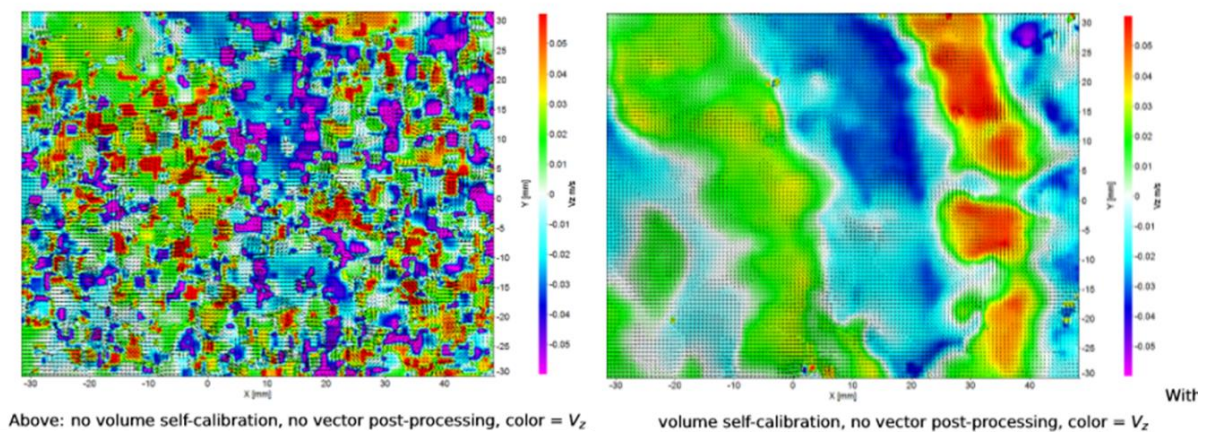
Figure 9 photos without (left) and with (right) volume self-calibration from product-manual of Davis 8.4 software

Volume reconstruction (fast MART)

As described in the theory of stereoscopic PIV, MART is introduced. Thanks to the great improvement in computer memory, multiplicative line-of-sight (MLOS) estimation combined with the usage of simultaneous implementation of multiplicative algebraic reconstruction technique (SMART) is used to provide fast and precise volume reconstruction.

MLOS estimation can determine possible locations of particles in the volume (C. Atkinson and J. Soria 2009). Once the arrangement of data is collected from the MLOS approach, every voxel is corrected based on the simultaneous projection to every pixel.

$$I_j^{k+1} = I_j^k \prod_i^{N_i} \left[\left(\frac{P_i}{\sum_n W_{in} I_n^k} \right)^{\mu w_{ij}} \right]^{1/N_i} \tag{5}$$

Where N_i is the total number of pixels observed in the given voxel j.

The application of MLOS-SMART has proved to reach up to 15 times of the speed that traditional MART can achieve within 5 iterations. The drawback is that the amount of computer memory should be enough for the storage of data.

Extract intensity z-profile

This step is aiming to estimate the quality of reconstruction volume. The result should look like the following picture where the red and the green profile indicate the result from different frame.
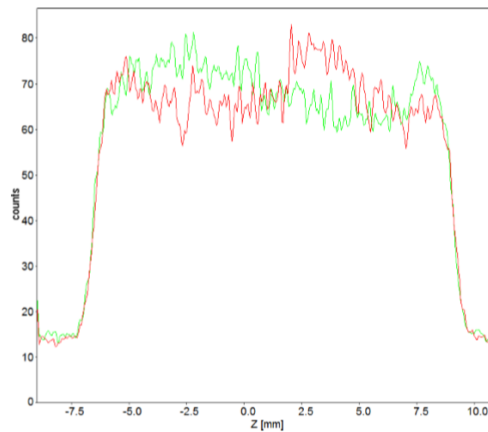
Figure 10 Estimated z-profile for extract intensity from product-manual of Davis 8.4 software

Volume correlation

In DaVis software, the volume correlation algorithm which is based on FFT technique performs faster. There, you can adjust the parameters for correlation volume and multi-pass postprocessing. In correlation volume window, selecting a smaller sub volume and unselecting the volume in the direction which should be reduced save much time on calculation. Each pass should be post processed in order to be stable. Some filters which define the range where vectors out of it will be disabled. Some other ways for multi-pass postprocessing are *fill up all*, *smoothing*, and *polynomial filter*.

Motion tracking enhancement (MTE)

As mentioned above, ghost particles are formed when the cameras capture the intersection of particles. The principle of MTE is to consider the recordings from two cameras or more (in this case, two cameras) as the same group of particles. With the help of known flow field, the ghost particles will be eliminated if the corresponding locations recorded at t1 do not fit the particle locations recorded at t2 (Matteo Novara, and Fulvio Scarano, 2010).

Sequential motion tracking enhancement (SMTE)

In MTE calculation, the knowledge of reconstructed intensity and the velocity field is required. This way of evaluation is regarded as a time-sliding-kernel approach (K. P. Lynch and F. Scarano, 2015). However, to increase the accuracy, the size of temporal kernel should also increase resulting in the higher cost. SMTE approach calculates the sequential motion of particles in terms of the previous two reconstruction, so-called *time-marching* algorithm. In practical work, two suggestions should be bore in mind. First, the value of extrapolation of the object intensity should not be zero. Second, the beginning two snapshots should be reconstructed by MART algorithm. Overall, SMTE approach demonstrates two better portraits than MTE, higher accuracy of enhanced guess and lower cost.

2.3.3 TSI Insight 4G™ software

Dynamic Masking

It usually refers to the analysis of shapes within images. This technique can create a mask for object in an image automatically. In other words, without the knowledge of object shape, movement direction, or speed can also process the data. However, the mask is the overlap between images, causing the removal of some particles. The key factor that influence the outcome of dynamic mask is the contrast between objects and the flow field. Once the images are taken (raw image pair), switch to the greyscale mode, and then click on the darkest point on the image within the generated mask. If some dot appears in the image, adjust the threshold (as filter). Last, adjust the intensity restoration for better boundaries. Eventually, background noise can be removed.
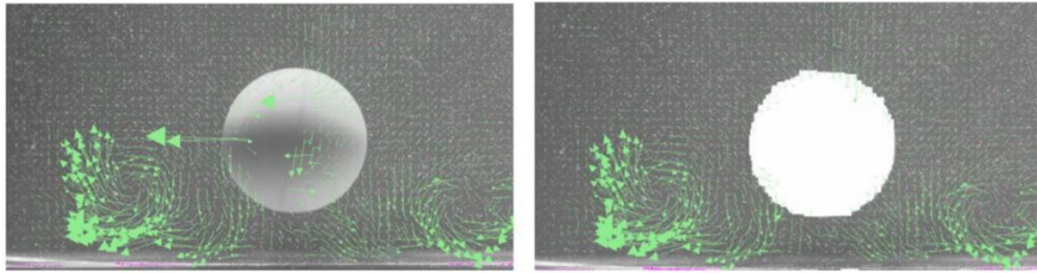
Figure 11 Dynamic masking removes large, non-physical vectors in masked regions from TSI APPLICATION NOTE PIV-018

Uncertainty Analysis: ***Primary Peak Ratio (PPR)***

The PPR is the ratio between the primary correlation peak to the second tallest peak. With this method, the uncertainty of PIV measurement can be predicted regardless of containing prior knowledge of image quality and local flow condition or not. This relationship exhibits better performance for phase-only generalized cross-correlation PIV processing, while the standard correlation approach showed weaker performance (John J Charonko and Pavlos P Vlachos 2013).

3   **Method**

In this paragraph, the experiment conducted by stereoscopic PIV is described and the dimensions of parts in stereoscopic PIV and tomographic PIV are also addressed. However, the ultimate research is to conduct the similar experiment with two different PIV devices. In this master thesis, only the experiment with stereoscopic PIV is done and the one with tomographic PIV is described in the future work, which is undone yet, and we aim to discover some difference in the future work.

Dimension of parts for tomographic PIV

Camera – LaVision's Image sCMOS camera

Exposure time	
Number of pixels	2560*2160 pixels
Pixel size	6.5 μm * 6.5 μm
Active area	16.6 mm * 14.0 mm
Spectral range	370 – 1100 nm
Frame rate	50 fps
Operating temperature	10 – 40 °C

Laser- EverGreen HP (EHP15-340-S $\lambda \lambda \lambda$)

Specification	
Repetition rate	15 Hz
Pulse energy	340 m*J
Pulse width	<15 ns
Energy stability	<2 % rms
Beam diameter	<10 mm

Laser Timing Stabilizer

Specification	
Wavelength range	300 – 900 nm
Max. Beam diameter	19 mm
Temporal resolution	1 ns
Lower detection limit	2.5 mJ / pulse
Operating temperature	50 °C

3.1   **Research Design**

For stereoscopic PIV

This experiment is done in the laboratory of fluidmechanic in technical university in Liberec. The overall appearance of this experiment is shown in Figure12. Firstly, the calibration target (21cm*21cm) is set aligned with where the light sheet should be emitted. Also, the vessel is placed with an angle at 45 degrees as it is aimed to be parallel to the lenses of cameras because in other case the refraction of the vessel should be taken in account. In addition, the rest two sides of the vessel are covered with black papers in order to reduce the interruption from outer light sources as the experiment is done in the dark environment where the reflection of the laser beam from tracing particles can be observed much clearly. Two cameras are set from both sides at an angle of 45 degrees with angular displacement, and the small angle, which is nine, between the cameras and the lens planes are adjusted according to the resolution of images. As a consequence, many steps need to be done before the suitable degree for this experiment is found. The fundamental technique for stereoscopic PIV to get the third axis is based on the calibration in z direction. To define the coordinate system, calibration images are recorded in five different position (figure 13).
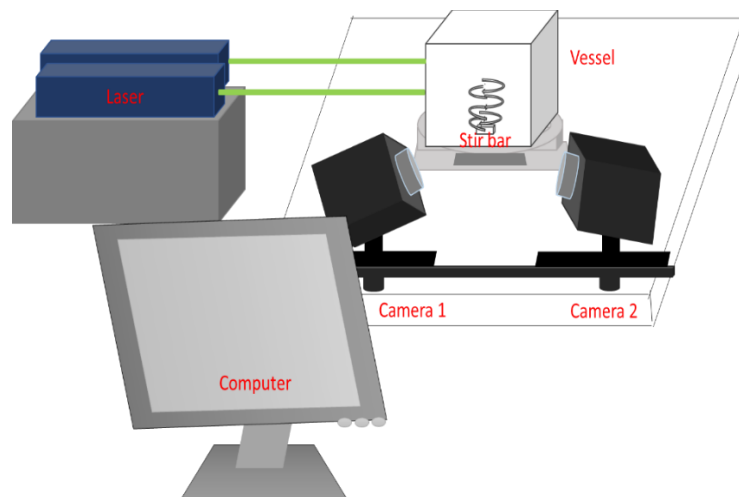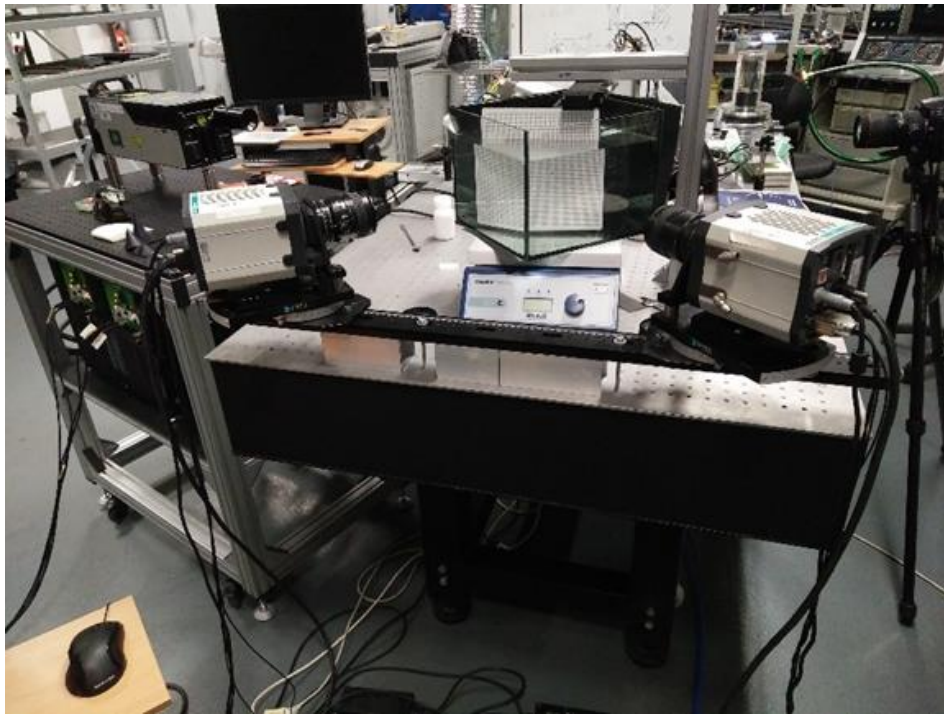

Figure 12 Schematic of experiemnt setup

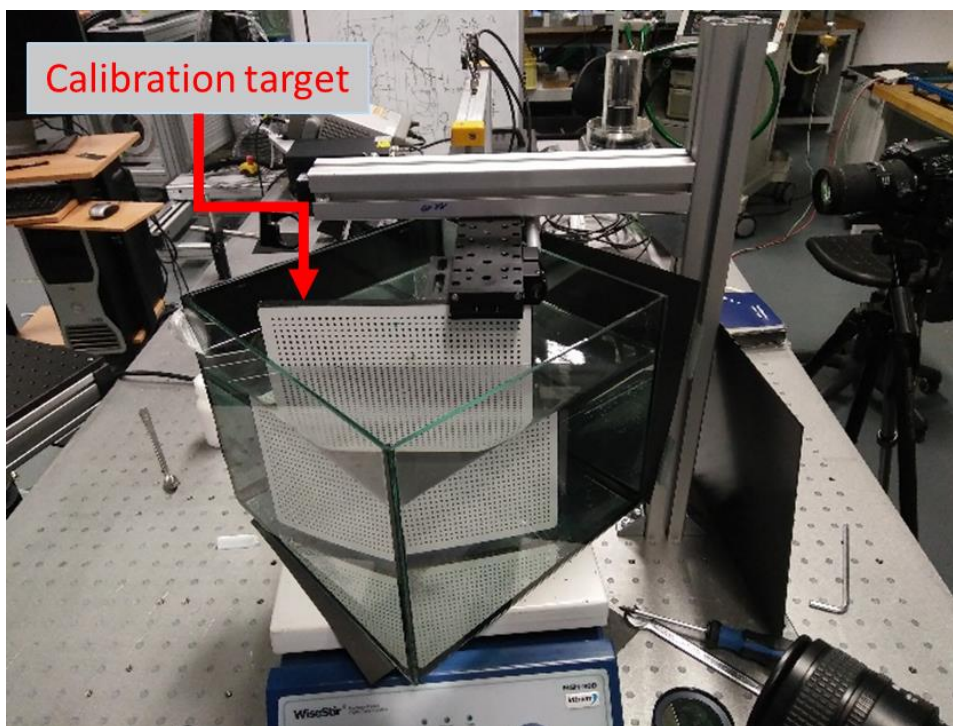*Figure 13 General view of setup equipped with Stereo-PIV*

Figure 14 Vessel with calibration target in it

In figure 14, the vessel with calibration target and the recording cameras are shown. In figure 14, PIV setup is shown. CCD chips are tilted at small angle with respect to the light sheet plane produced by laser light. Scheimpflug adapter is used to focus on the particles in the image plane.
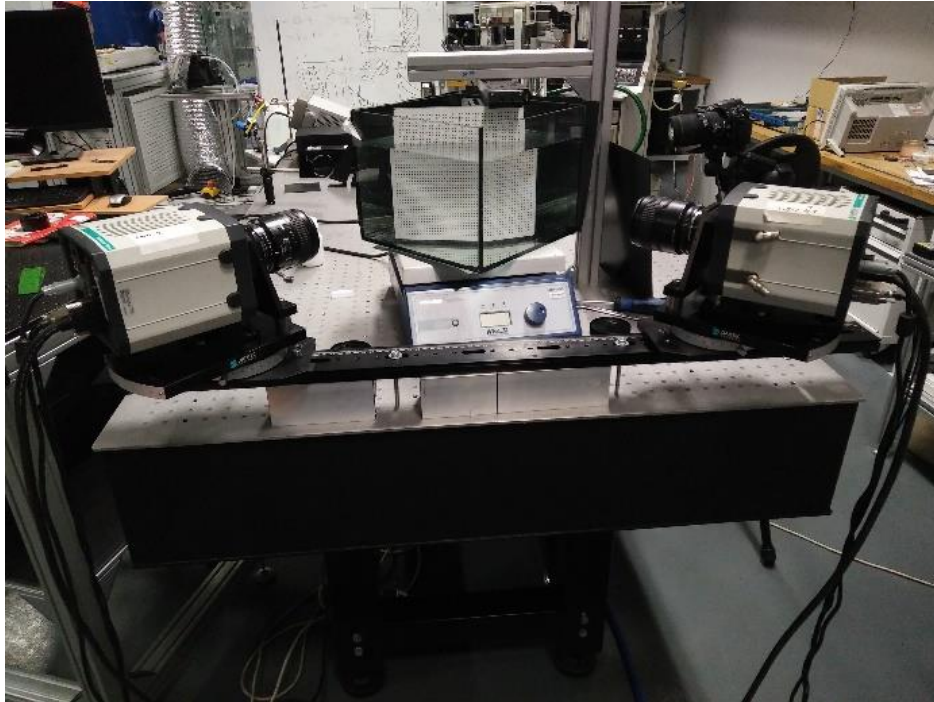
Figure 15 Configuration of the set-up during calibration

The first one is set to be the original point and the other four images are taken 1mm, 2mm in front of the original point and 1mm, 2mm away from the original point. Till this step, the calibration work is finished. As the interface is shown as followed figure15.
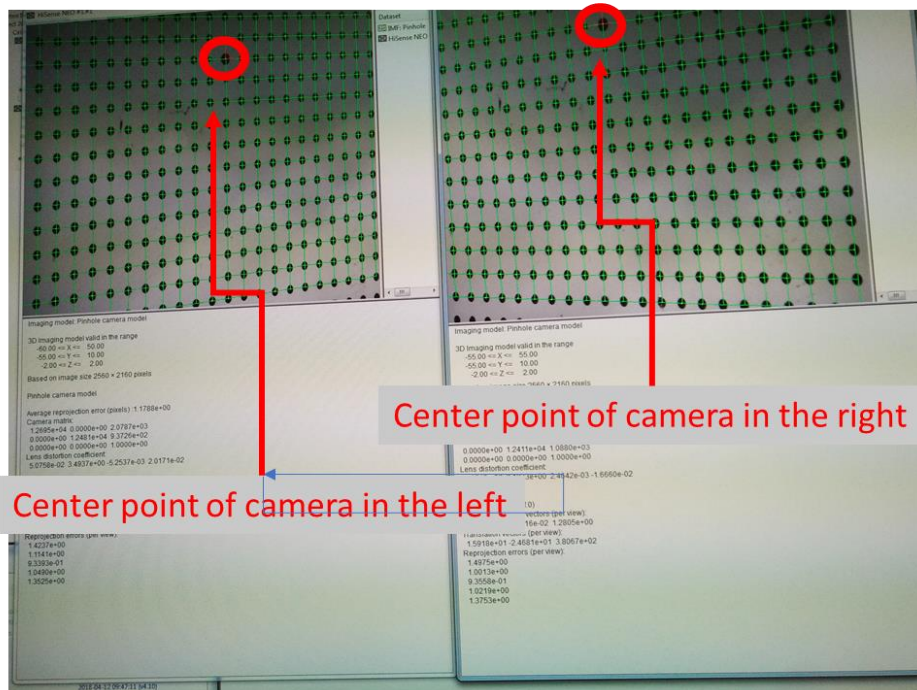

Figure 16 Interface of calibration in Dantec's software

After the addition of tracing particle, the stir bar is put into the vessel which is covered with black papers from two sides to reduce the influence of other light sources in the laboratory. The rotation speed then is 200 rpm. The tracer particle is PA with 20 μm in diameter (fig.17). The time between two pulses is 2000 μs. Number of images is 100. After the data is collected, the rotation speed is increased into 500 rpm, and the mentioned procedures are repeated again.
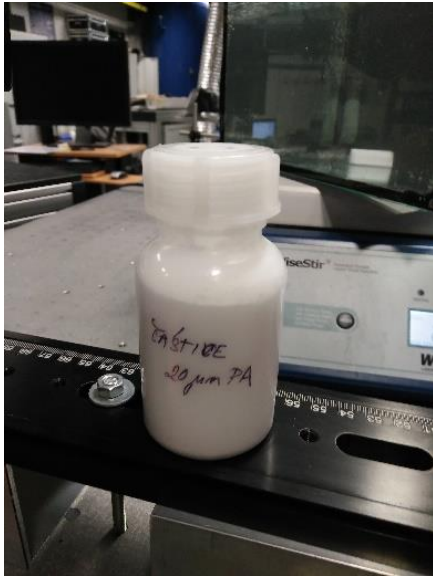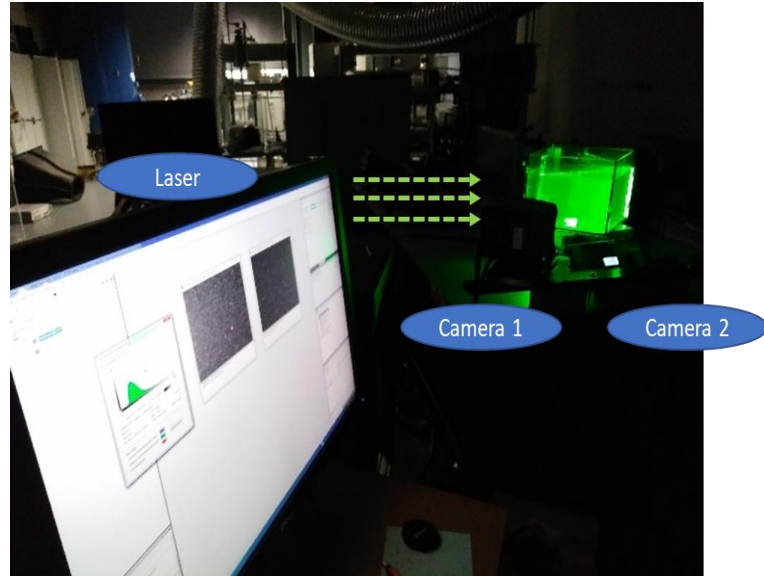

Figure 17 used tracing particles

Figure 18 The photo taken during the experiment

4 Results

The motions of fluid in the vessel with 200 rpm and 500 rpm are recorded in order to test the performance of stereoscopic PIV in comparison to the future experiment which will be done by tomographic PIV. The time between two laser pulses are set to 2000 microsecond and the number of images is 100. From these 100 images, 12 images are selected to describe the motion of fluid in the vessel.

4.1 Research findings

In order to obtain more information about the flow field generated by the stir bar, we first captured PIV data with 200 rpm (figure 19). With 200 rmp of magnetic stir bar. The diagrams are exported directly from DynamicStudio; thus, the scale is not added. The purpose of them is to give the general motion under different rotation speed. From figure 19, we can discover the formation of vortex whose size varies from time to time and out-of-plane vectors are formed on both sides. In the figure 19 and figure 20, the general movement of flow is shown.

These two velocity maps are originally exported from DynamicStudio software and then calibrated with its vector maps in Tecplot. The orange colour describes the inward motion and blue colour describes the outward motion. However, the stir bar is put near the centre of the vessel. The image plane does not match the centre of the stir bar completely. Thus, in the centreline, where coordinate x is zero, vortex does not appear in each picture. The instantaneous velocity contours in figure 19-c, and figure 19-l show the presence of periodical structure of vortex formation. Figure 19-a depicts the formation of in-plane vortices near centreline on the top and the bottom. Gradually, these vortices come closer and eventually connect to each other, forming a vertical top-to-bottom vortex (figure 19-g). the column-like vortex is thinner and manifests the maximum inward motion. After the connection of vortices, it once again divides into a few smaller vortices as in figure 19-j. In short time, these vortices reform into a column-like vertical vortex in figure 19-l. Nevertheless, it is seen that the out-of-plan vortices follow the similar change with inward vortex. It is found that in figure 19-j, there are two small inward and outward vortices on the bottom near the centre. As inward and outward motions are observed in figure 19, it indicates the contraction and expulsion phases in between. The velocity distribution is found to be asymmetrical near the centre.
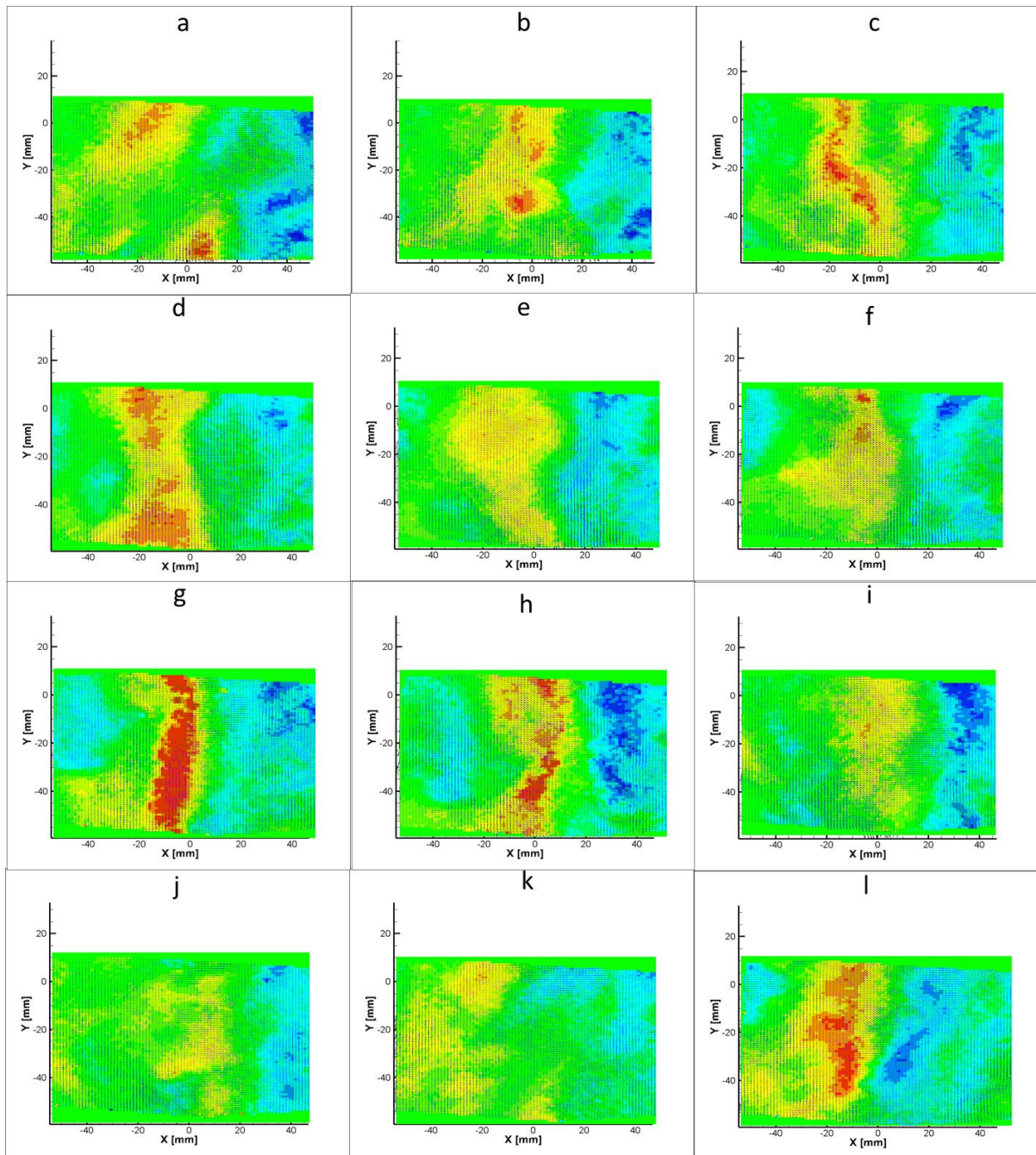
Figure 19 Instantaneous velocity map at 200 rpm exported from DynamicStudio software

In figure 20, due to the higher rotation speed, at initial stages, formation of smaller vortices is observed. Unlike the phenomena appeared in figure 19, where vertical vortex is formed periodically, in figure 20, the mentioned phenomena is not indicated since the formation appears in figure 20-l only. Furthermore, due to the higher rotation speed, the movement of vortex in z-axis is suggested to move more aggressively, explaining the less observed vortices

from figure 20-e to figure 20-f as the vortices move out of the observed plane range. Also, higher rotation speed, the effect from boundary should be taken into consideration.
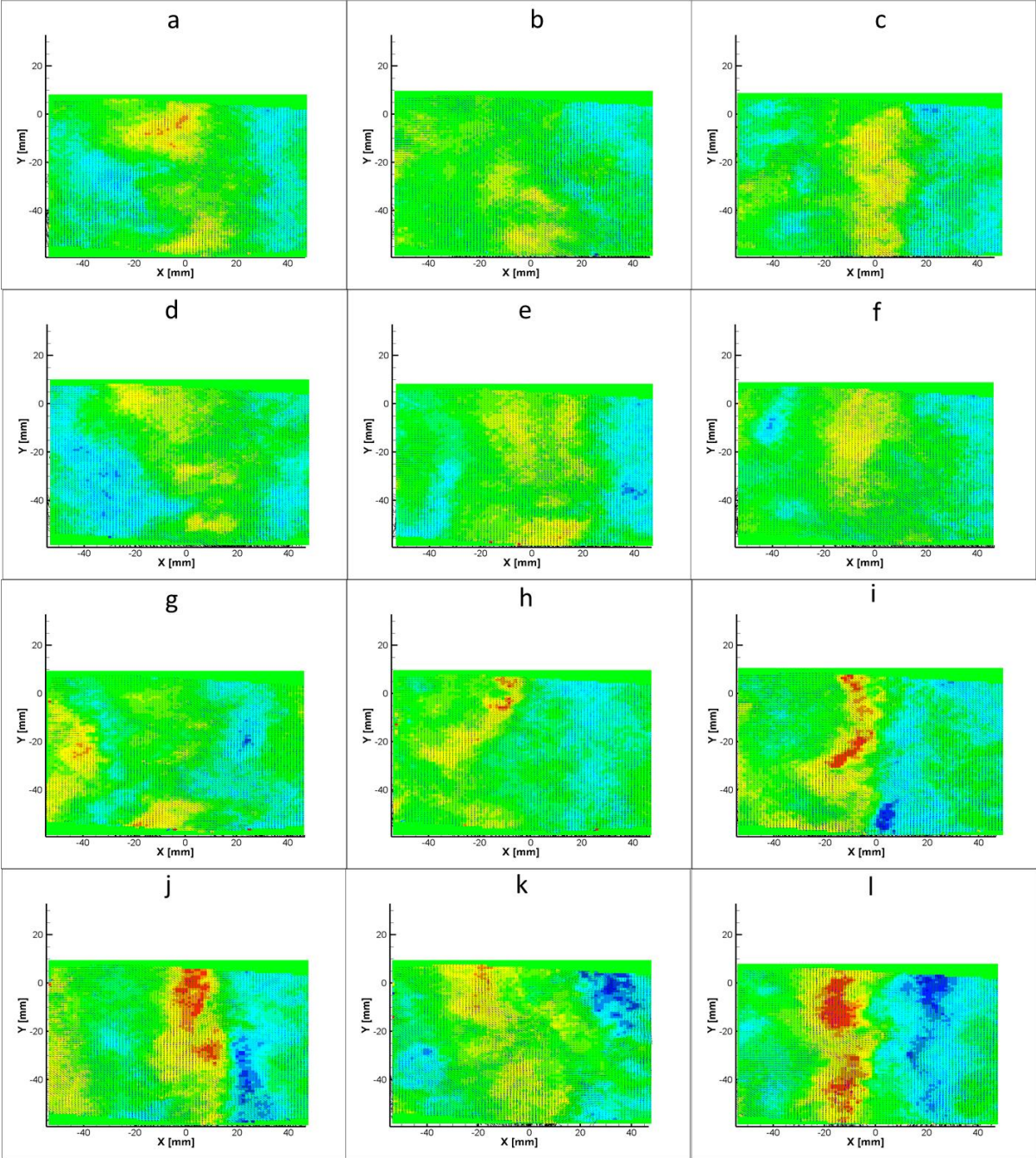

Figure 20 Instantaneous velocity map at 500 rpm exported from DynamicStudio software

Furthermore, the movement of flow field in 3D contour is shown in figure 21 and figure 22 with data exported from DynamicStudio and draw in Tecplot. The images are picked up in serial; thus, the continuous change of fluid can be observed. The mean velocity contours of U

are shown. The contour legend depicts the U velocity, ranging from -0.02 to 0.02 m/s. It should be mentioned that the in-plane velocity prevails near the centre. As depicted below, the maximum U velocity moves along x-axis forwards and backwards. The creation of vortex matches the 2D velocity maps. The vortex is not stable.
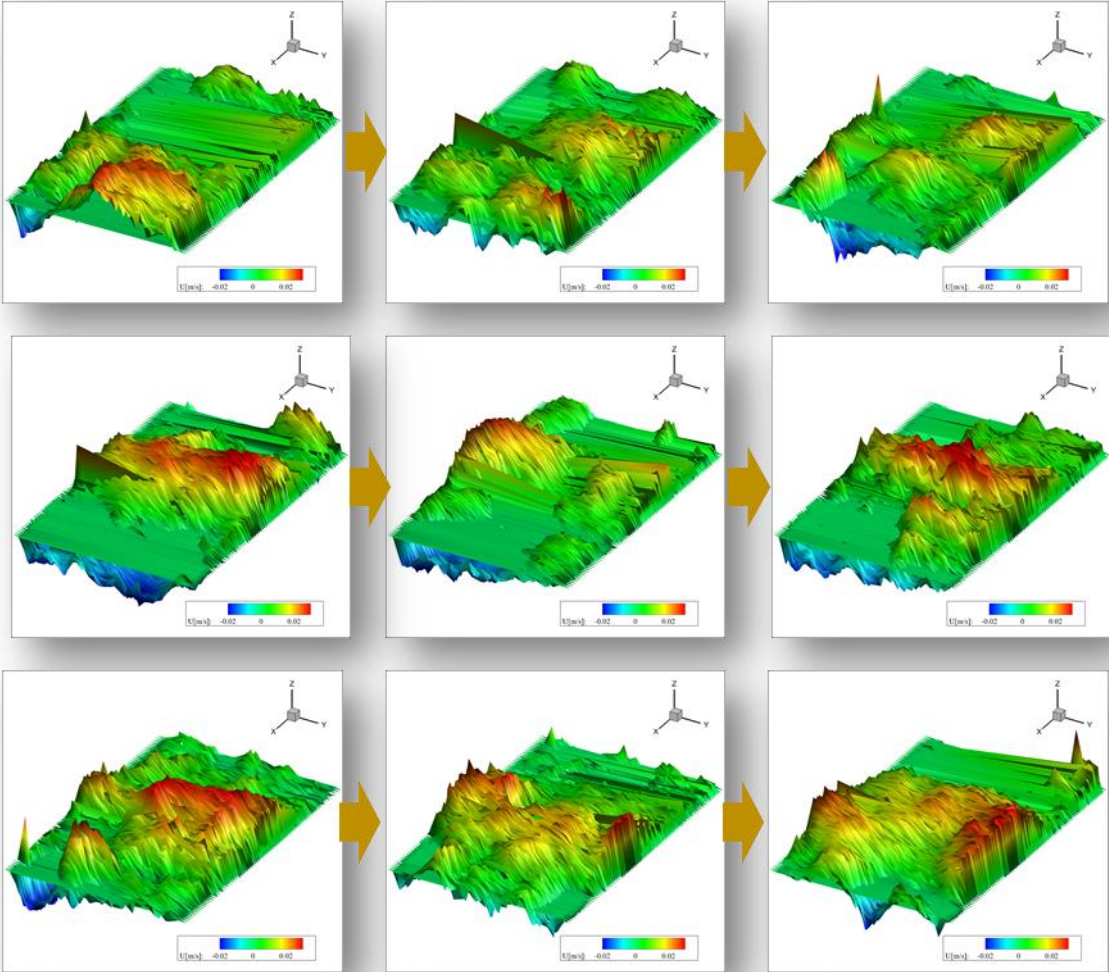

Figure 21 3D reconstruction of instantaneous velocity contoursat 200 rpm

The amplitude of peaks shown in figure 22 is obviously higher and more severe than the one in the previous condition. The contour legend depicts the U velocity, ranging from -0.08 to 0.09 m/s. The prediction of out-of-image-plane is proved in 3D contours as the movement in z-axis is more obvious. These movements seem to be too severe. In this case, 3D PIV may perform better recording as it contains much information in other dimension.
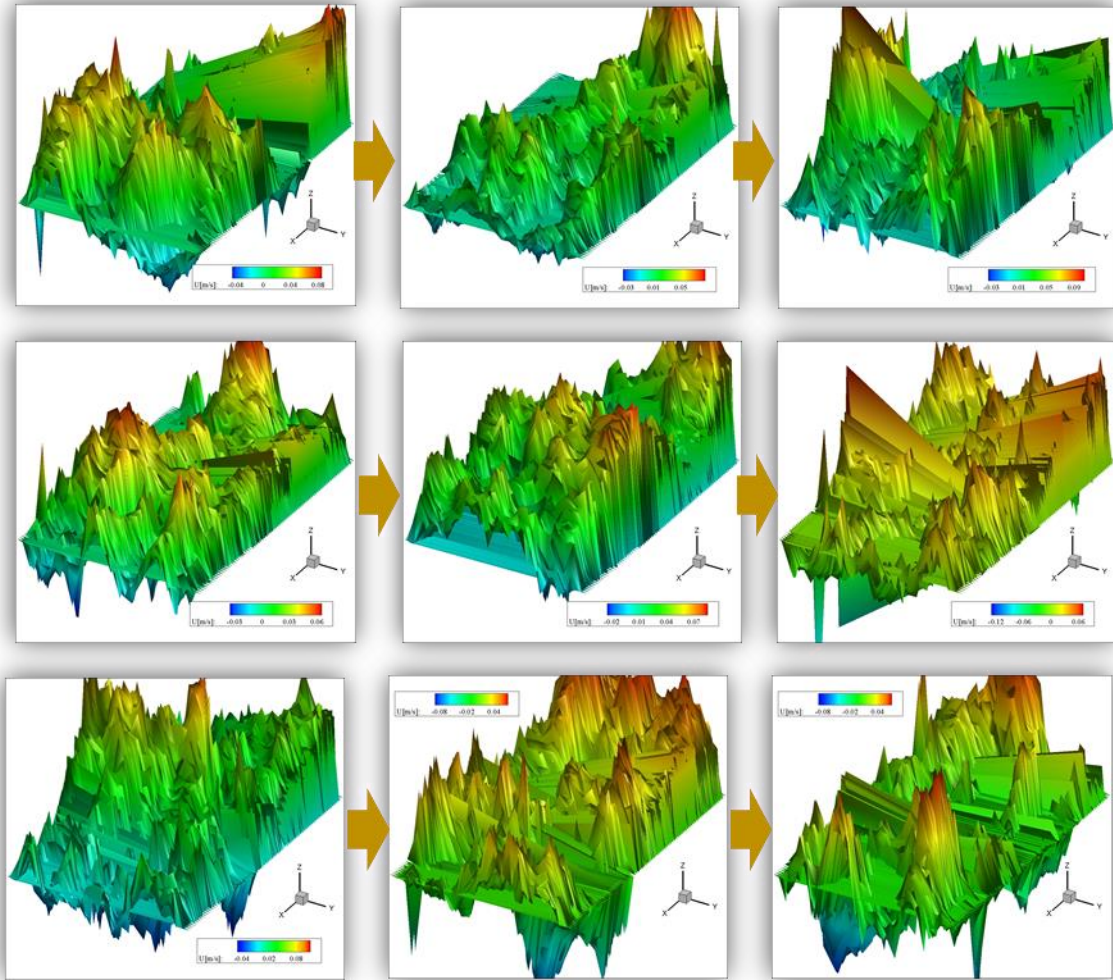
Figure 22 3D reconstruction of instantaneous velocity contoursat 500 rpm

POD (section 2.3.1) methods is usually implemented and applied for analysing complex unsteady flows in practical work. POD decomposes a set of instantaneous velocity fields into a modal base as depicted in figure 23. In this work, POD is carried out using snapshot method. Velocity fields are extracted directly from the measurements. As a result, eigenfunctions and the associated eigenvalues can be obtained. Then the required instantaneous velocity field can be projected according to each POD eigenfunction. First few eigenmodes can be used to completely describe this flow field, since they contain most of the total energy. Aside from first few eigenmodes, figure 23 also shows how each mode has slightly different in energy.
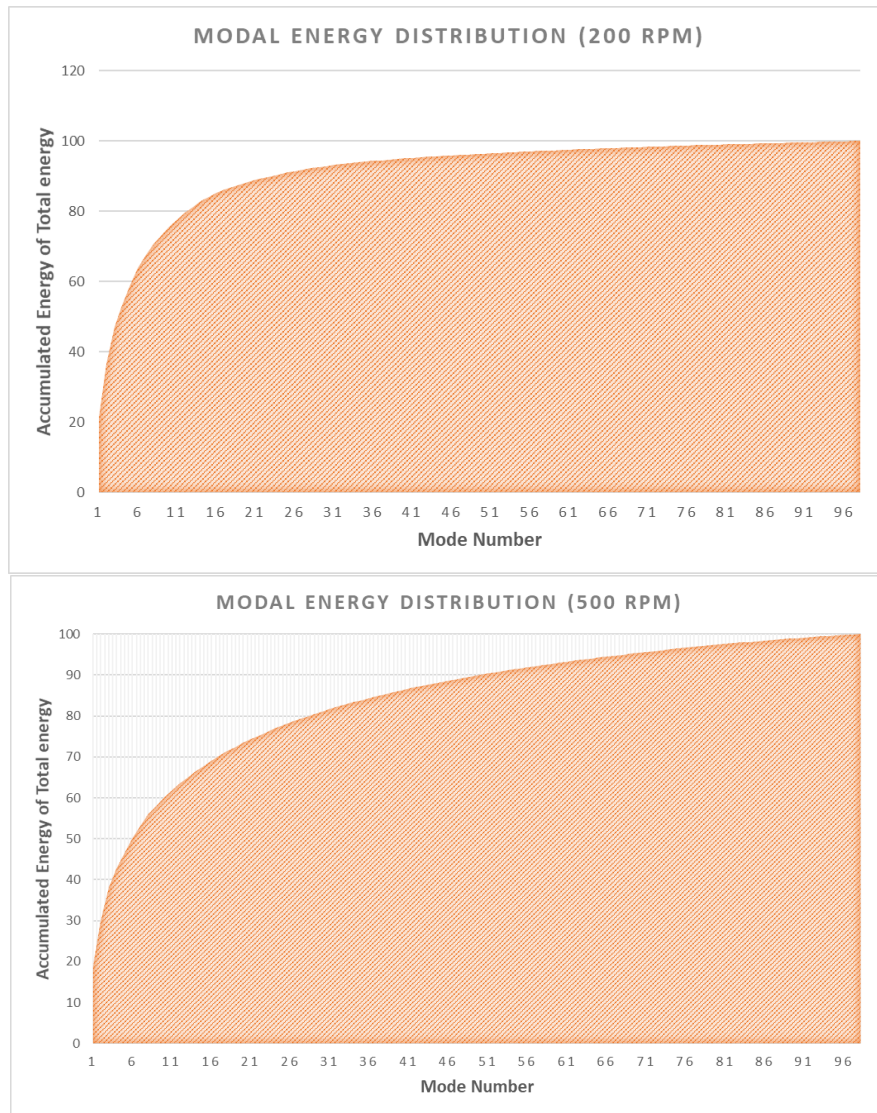
Figure 23 Modal Energy Distribution

The main feature of POD method is the reconstruction of dominant structures of a complex flow field without losing the time dependency of the data, minimal measurement errors, and simulation of missing. Therefore, results from POD method is compared here. POD projection data is exported from DynamicStudio and then used to draw the diagrams in figure 24 and figure 25. In figure 24, snaps in different orientation view are shown. In both figure 24 and figure 25, pictures are selected when column-like vortex exists. The contour legend depicts the U velocity in both figures, ranging from -0.016 to 0.008 m/s, which is slightly smaller than in the previous figures. However, when processing a huge amount of data in advance experiment, POD is preferred as it can reduce the processing time, yet still offering good quality of prediction in instantaneous velocity fields.
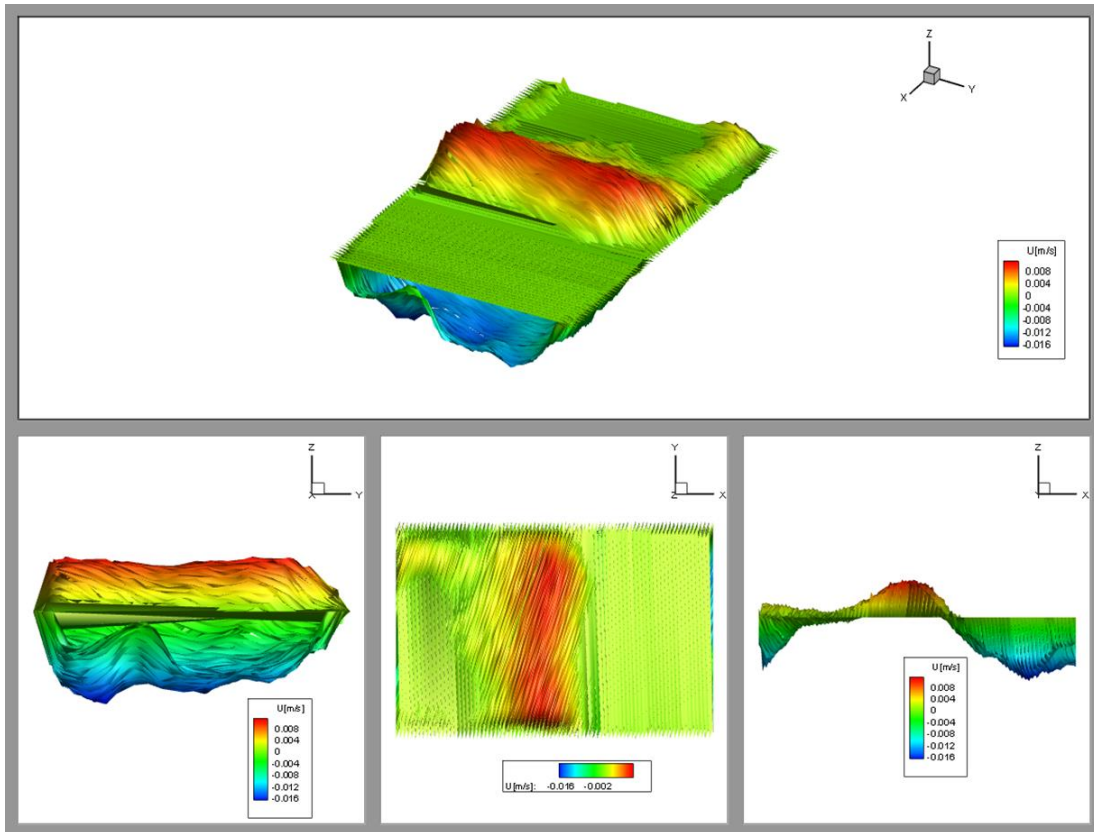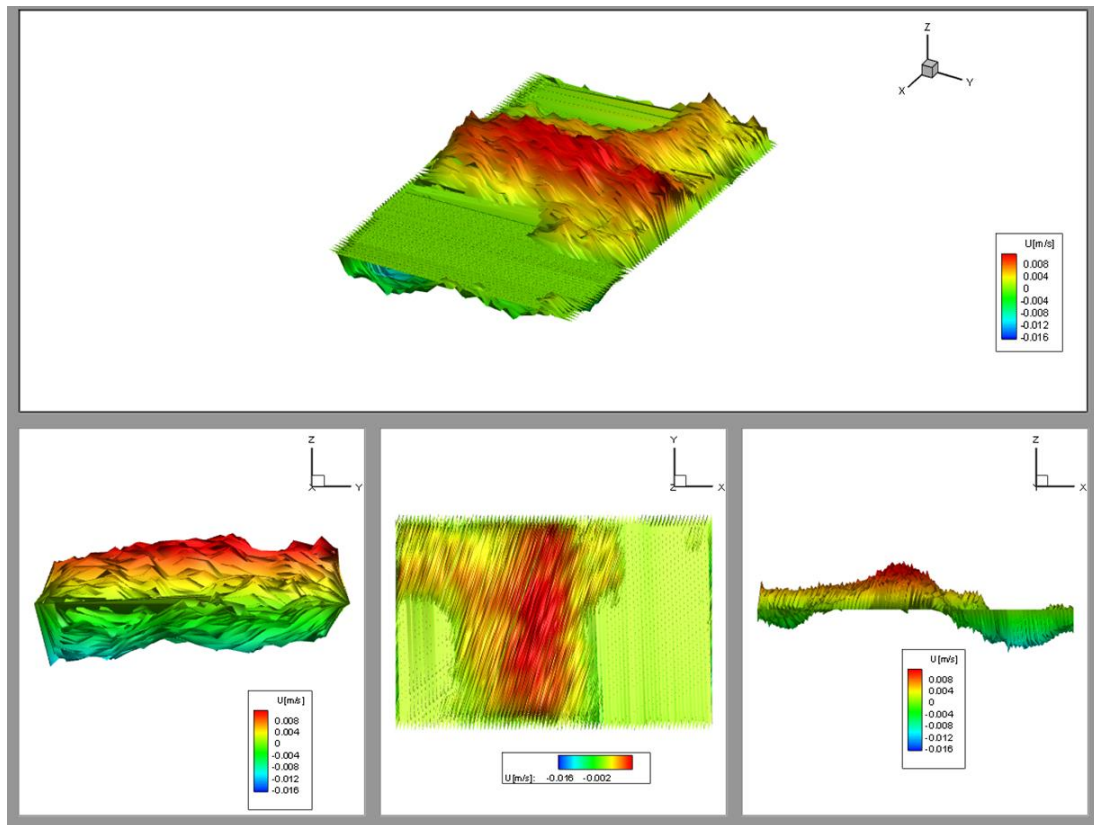
Figure 24 POD projection at 200 rpm

Figure 25 POD projection at 500 rpm

4.2 Brief Comments on the Results

Usually, the birth of a vortex is due to the dramatical change in the structure of pathlines near the stagnation points. There are three ways of formation of vortices, – inside the flow, from free surface, and from wall. Near the top of the vessel, vortices can be born (figure 21) from gas-liquid interface as the split from single stagnation point into multiple stagnation points. Those associated boundary conditions are investigated in previous research (Jaewook. Nam et al. 2009). The nature of the mean velocity field is not properly proved here as the stir bar might not be located exactly at the centre of the vessel. As the comparison of rotation speed at 200 rpm and 500 rpm, these results indicate the larger velocity fluctuations driven by the rotating magnetic stir bar. However, the unsteady flow motion is suggested to be the result of temperature or viscosity difference (T. Syuto et al. 2010), which are not considered in this experiment. It is worth mentioning that the fluctuating velocity field may be the result of the difference in turbulence intensities (T. Gono et al. 2012) near the inducing magnetic force.

From the experiment, POD method is implemented owning to its key advantage at solving the problem of insufficient computer capacity. Also, as PIV is advantageous in taking the instantaneous images of flow structure, making it a good tool for the description for understanding of the large-scale unsteady motion. With POD, huge amounts of high-dimensional data can be processed with descriptions into low-dimension. However, with this method, one-dimension feature may be neglected. In addition, in our experiment, we fixed the coordinate system, so the effect of sensitivity to the change of coordinate system of POD method could be lighter. Figure 23 shows the convergence of the accumulated eigenvalues. Till the sixth eigenvalue, it contains nearly 50% of total energy. Compare to the previous research (Laurent Graftieaux et al. 2001) which converges faster than this experiment, the author suggests the existence of low-order dimension may be the cause. Moreover, when POD projection is applied, one thing should be borne in mind is the problem to gain the information with particles "*travel quickly with little extension in space*" (Markus Muller 2006). However, POD method provides good quality of dynamic information as shown in figure 24 which can be compare with figure 20-g, and in figure 25 which can be compared with figure 21-l.

5   **Conclusion and Recommendations**

In this research, the comparison in performance and performance should be mentioned between existing stereoscopic PIV and the upcoming 3D PIV. The principle of PIV is introduced in chapter one to offer readers the fundamental idea how PIV is composed and works. The introduction of components is also included, such as light sources and tracing particle. State-of-the-art section narrates the trends in PIV related researches, mostly focusing on tomographic PIV. Next, the preparation of experiments with PIV should be done, such as calibration. More cameras are used, more complicated calibration procedures need to be done. Under the common proposed concept, PIV apparatus is produced by various companies, Dantec, LaVison, and TSI. As a consequence, the processing software contains different interfaces and functions. Here, the basic functions are depicted. Since the stereoscopic PIV in faculty of mechatronics uses Dantec system, DynamicStudio software is thereby used. This preliminary experiment aims to test the performance of stereoscopic PIV, showing what this system can achieve. When the newly-bought 3D PIV is delivered to the department, the further testament of this system will be checked, and the simple experiment will also be prepared.

This chapter will mainly be divided into two parts. In first part, the overview of this study will be narrated. Then, in the second part, the future work about new device will be described.

5.1　Conclusions

Firstly, the historical background of PIV is described for example, based on the concept of Laser Speckle Interferometry, PIV is invented. Then the progress of such devices as well as the related techniques are mentioned such as Digital Image Correlation and Background Oriented Schlieren Technique. The theory section, however, targets on introducing the displacement of cameras and calibration work which has to be done in stereoscopic PIV before each experiment, which shares similar idea with 3D PIV. Therefore, in theory of tomographic PIV, basic reconstruction algorithms are then described. The aim of this study has been considered to provide the readers the general idea how to conduct the experiment, for instance, the calibration procedures in order and the possible analysis of PIV from the existing system; furthermore, to analyse the common phenomena happing in daily life such as swirl in static lake. In other words, this study is to provide some information and do the preliminary experiment as to get familiar with the system as the future assembling and testing work with 3D PIV system. As the result shows, the formation of vortices is observed. In chapter three, practical work in the laboratory and the real setup of the experiment are shown. Based on that, Teclpot is used to sketch the flow structure. Also, though the vortices appear, different rotational speed is assumed to also cause different influence in the flow. Thus, experiments with 200 rpm and 500 rpm are conducted and compared. In previous research, different Reynold numbers or viscosities numbers are discussed. These parameters can be induced in the future work. In 3D PIV, the device which collect larger amounts of data from multiple cameras, the processing time for "snapshots" of dynamic fluid will be greatly increased. Nowadays, different algorithms are developed. In this study, POD method has been implemented and used to generate the velocity maps changing with time. Through this study, one can get familiar and gain the overall concept towards any experiments related to PIV device.

5.2 Recommendations for Future Research

In the future work, the experiment is planned as follow. As the comparison, the experiment should be in the consistent setup. It means that the same size of vessel will be applied and the same parameter will be adjusted.

An octagonal tank with 20 cm at each side and 50 cm at its height will be filled with pure water as a way to reduce the effect from impurity. The temperature will be controlled and held constant. Four cameras will be arranged to observe the motion of particles fr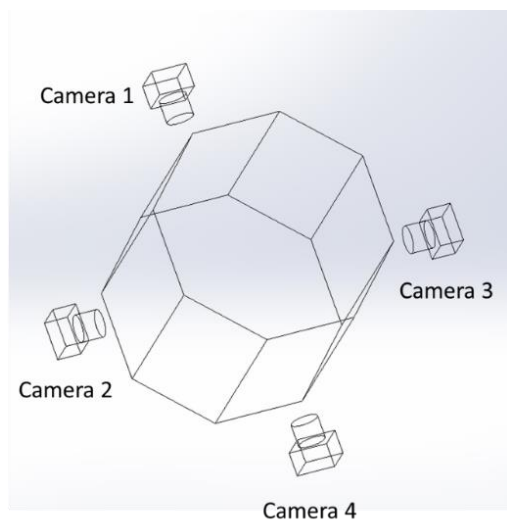om four different angles adapted in Scheimflug condition. Glass hollow spheres with mean size from 9 μm to 13 μm seeding particles will be used as tracing particles together with 340 mj Nd:Yag laser, which generates the light sheet from sides. The light should be introduced parallel to the glass and perpendicular to the circulating stream. Also, adjustable mechanical aperture should be equipped to define sharp borders within the measurement domain. The system was synchronized with a LaVision Programmable Timing Unit (PTU X) controlled by the DaVis10 software. The interrogation window will be set at 8 x 8 x 8 voxel and 75 % overlap as it shows more accurate detection. Four 5.5-megapixel cameras record a field of view of 50 mm x 50 mm. The sCMOS cameras are in 2560 x 2160 pixels. The stir bar as a driven force will then be placed at the centre of the tank. The number of particle (particles density) can be calculated by the software according to the interrogation volume. 3 series of 1000 images will be recorded. Each series should contain the flow filed maps under two different rotational speed, 200 rpm and 500 rpm. The laser will be turned on after the stir bar reaches stable rotation. Each set of data will be collected as a comparison to the one with stereoscopic PIV. However, as the powerful device for recording instantaneous volumetric images, 3 series will have different thickness light sheet, and the corresponding particle density should be altered. In reconstruction and cross-correlation procedures, first particle locations are reconstructed in the 3D volume by FastMART algorithm. Secondly, the cross-correlation is performed with 75% overlap for different volume sizes. Usually, interrogation volume should be set in bigger voxel initially as to obtain a rough estimation of the velocity field, and then set in smaller voxel. Comparing the results from different volume size, the most suitable interrogation volume should contain

Figure 26 Imganiary Experiment for Tomo-PIV

sufficient information without losing too much accuracy. The velocity profile with vortex in 3 dimensions is predicted to obtain and be used to compare with the previous experiment.

The result from tomographic PIV is expected to show the qualitative agreement with the one from stereoscopic. Even the more accurate result is expected from 3D PIV. The aim is to contribute to an enhancement of the understanding of PIV system. In the future, especially, 3D PIV will definitely be in use amongst wide ranges. All these measurements would only be efficient and time-saving when the requisite knowledge is drilled in operators.

Bibliography

C. H. Atkinson, C. J. Dillon-Gibbons, S. Herpin, J. Soria (2008) Reconstruction Techniques for Tomographic PIV (Tomo-PIV) of a Turbulent Boundary Layer

C. Aikinson,and J. Soria (2009) An efficient simultaneous reconstruction technique for tomographic particle image velocimetry

F.Alberini,, L.Liu, E.H.Stitt, M.J.H.Simmons (2017) Comparison between 3-D-PTV and 2-D-PIV for determination of hydrodynamics of complex fluids in a stirred vessel

Feng Bao, iun-Jih Miau, and Tzu-liang Chen (2007) Journal of Aeronautics, Astronautics and Aviation, Series 8, Vol.39, NO.2, pp.093 - 098 PIV Technique and its Application in Fluid Measurement

Anindya Chatterjee (2000) An Introduction to the Proper Orthogonal Decomposition

John J Charonko and Pavlos P Vlachos (2013) Estimation of uncertainty bounds for individual particle image velocimetry measurements from cross-correlation peak ratio

G.E. Elsinga, F. Scarano, B. Wieneke, B.W. van Oudheusden (2005) Tomographic particle image velocimetry

Sijie Fu, Pascal Henry Biwole, Christian Mathis (2016) Numerical and experimental comparison of 3D Particle Tracking Velocimetry (PTV) and Particle Image Velocimetry (PIV) accuracy for indoor airflow study

Laurent Graftieaux, Marc Michard and Nathalie Grosjean (2001) Combining PIV, POD and vortex identification algorithms for the study of unsteady turbulent swirling flows

T. Gono, T. SyutoT. Yamagata, N. Fujisawa (2012) Time-resolved scanning stereo PIV measurement of three-dimensional velocity field of highly buoyant jet

Michael J. Hargather, Gary S. Settles (2010) Recent Developments in Schlieren and Shadowgraphy

F. Klinge, T. Kirmse, J. Kompenhans (2003) Application of quantitative Background Oriented Schlieren (BOS): Investigation of a wing tip vortex in a transonic windtunnel

C. J. Kähler, S. Scharnowski, C. Cierpka (2012) On the uncertainty of digital PIV and PTV near walls

Ralph Lindken, Jerry Westerweel, Bernhard Wieneke (2006) 3D micro-scale velocimetry methods: A comparison between 3D-µPTV, stereoscopic µPIV and tomographic µPIV

Zeyu Li, Jinling Wang (2014) Least Squares Image Matching: a Comparison of the Performance of Robust Estimators

K. P. Lynch, and F. Scarano (2015) An efficient and accurate approach to MTE-MART for time-resolved tomographic PIV

N. McCormick, and J. Lord (2010) Digital Image Correlation

Markus Muller (2006) On the POD Method- An Abstract Investigationwith Applications toReduced-Order Modeling and Suboptimal Control

Jaewook. Nam, L.E.Scriven, Marcio S., Carvalho (2009) Tracking birth of vortex in flows

M. Novara, and F. Scarano (2010), Performances of motion tracking enhanced Tomo-PIV on turbulent shear flows

D. R. Neal, A. Sciacchitano, B. L. Smith, F. Scarano (2014) Collaborative framework for PIV uncertainty quantification: the experimental database

N. J. Neeteson, S. Bhattacharya, D. E. Rival, D. Michaelis, D. Schanz, A. Schröder (2016) Pressure-field extraction from Lagrangian flow measurements: first experiences with 4D-PTV data

N. J. Neeteson, D. E. Rival1 (2016) A Finite Volume Method for Pressure Extraction on Unstructured Flow Data

Eric F. Oliveira, Sílvio B. Melo, Carlos C. Dantas, Daniel A. A. Vasconcelos and Luís F. Cadiz (2011) Comparison among tomographic reconstruction algorithms with a limited data

A. K. Prasad, and K, Jensen (1995) Scheimpflug Stereocamera for Particle Image Velocimetry in Liquid Flows

Bao Quan, Jiang Nan (2013) A Simplified 3D Reconstruction Technique For Tomographic Particle image velocimetry

Markus Raffel (2015) Background-oriented schlieren (BOS) techniques

T. Syuto. N. Fujisawa, T. Takasugi, T. Yamagata (2010) Flow visualization and scanning PIV measurement of three-dimensional structure in near field of strongly buoyant jet

C M de Silva, R Baidya and I Marusic (2013) Enhancing Tomo-PIV reconstruction quality by reducing ghost particles

A. Sciacchitano, D. R. Neal, B. L. Smith, S. O. Warner, P. P. Vlachos, B. Wieneke, F. Scarano (2014) Collaborative framework for PIV uncertainty quantification: comparative assessment of methods

Daniel Schanz*, Andreas Schröder, Sebastian Gesemann (2014) 'Shake The Box' - a 4D PTV algorithm: Accurate and ghostless reconstruction of Lagrangian tracks in densely seeded flows

Daniel Schanz, Sebastian Gesemann, Andreas Schröder (2016) Shake-The-Box: Lagrangian particle tracking at high particle image densities

L .K. Waters, G. J. Fix and C. L. Cox (2004) The Method of Glowinski and Pironneau for the Unsteady Stokes Problem F. Auteri, M. Carini, D. Zagaglia, D. Montagnani, G. Gibertini, C. B. Merz, A. Zanotti (2015) A novel approach for reconstructing pressure from PIV velocity measurements

A. Watanabe, H. Yokoyama, N. Ninomiya, H. Sugiyama, and D. Hitomi (2004) Camera Calibration Considering Scheimpflug Condition

Timothy W. Fahringer and Brian S. Thurow (2015) Comparing Volumetric Reconstruction Algorithms for Plenoptic-PIV
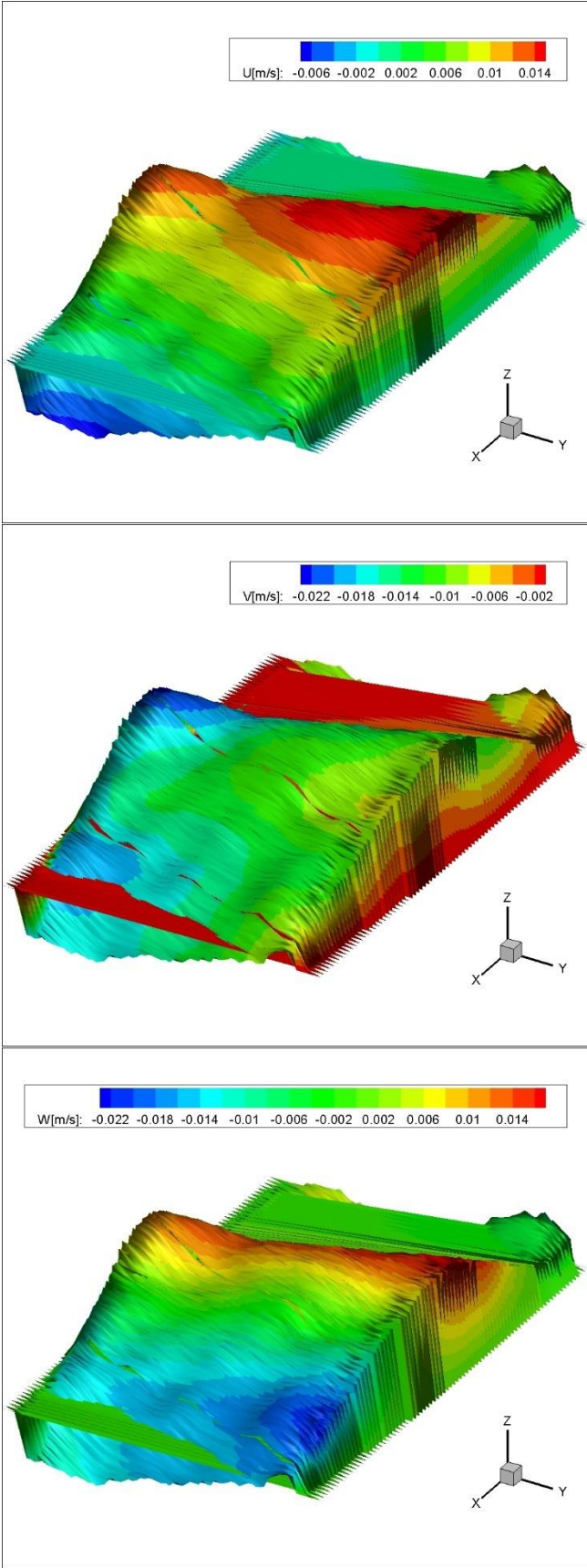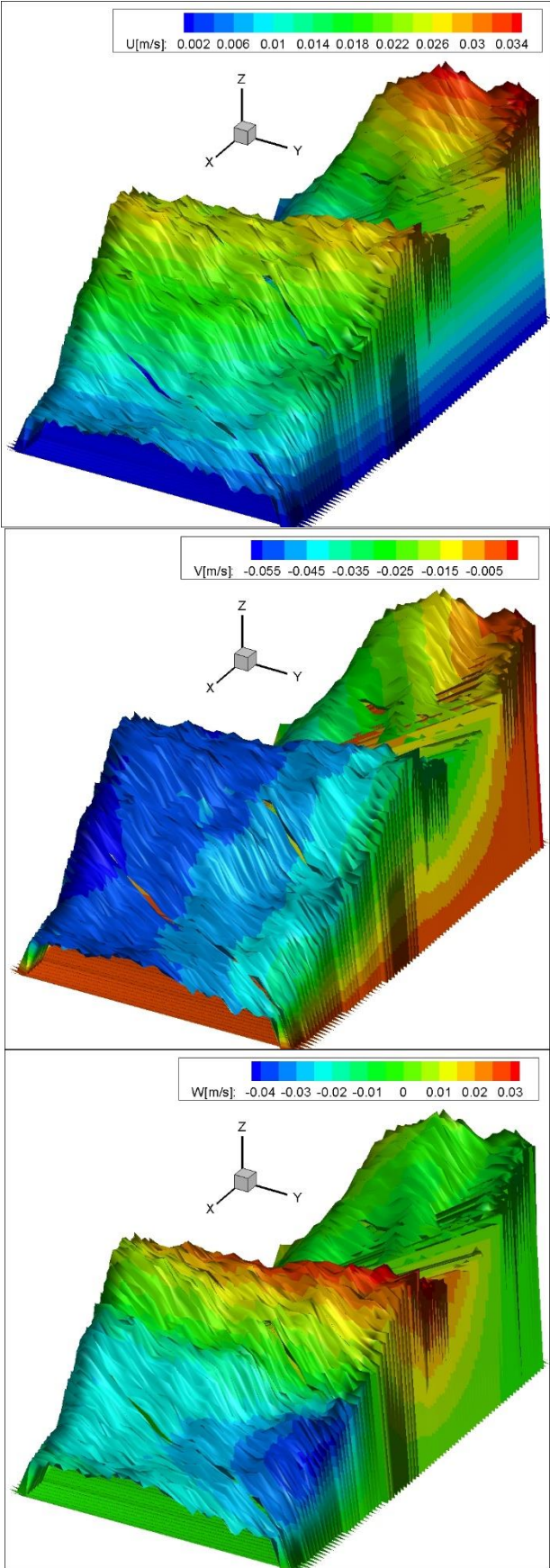
Appendix A

Figure 1 Vector statistic at 200 rpm

Appendix B

Figure 2 Vector statistic at 500 rpm